Title	Nuclear Localization of DNAJB6 is Associated with Survival of Patients with Esophageal Cancer and Reduces AKT Signaling and Proliferation of Cancer Cells
Author(s)	Yu, VZ; Wong, VCL; Dai, W; Ko, JMY; Lam, AKY; Chan, KW; Samant, RS; Lung, HL; Shuen, WH; Law, SYK; Chan, YP; Lee, NPY; Tong, DKH; Law, TT; Lee, VHF; Lung, ML
Citation	Gastroenterology, 2015, v. 149 n. 7, p. 1825–1836.e5
Issued Date	2015
URL	http://hdl.handle.net/10722/216802
Rights	© 2015. This manuscript version is made available under the CC-BY-NC-ND 4.0 license http://creativecommons.org/licenses/by-nc-nd/4.0/; This work is licensed under a Creative Commons Attribution-NonCommercial-NoDerivatives 4.0 International License.

Accepted Manuscript

Nuclear Localization of DNAJB6 is Associated with Survival of Patients with Esophageal Cancer and Reduces AKT Signaling and Proliferation of Cancer Cells

Valen Zhuoyou Yu, Victor Chun-Lam Wong, Wei Dai, Josephine Mun-Yee Ko, Alfred King-Yin Lam, Kwok Wah Chan, Rajeev S. Samant, Hong Lok Lung, Wai Ho Shuen, Simon Law, Yuen Piu Chan, Nikki Pui-yue Lee, Daniel King Hung Tong, Tsz Ting Law, Victor Ho-fun Lee, Maria Li Lung

PII: S0016-5085(15)01193-2
DOI: 10.1053/j.gastro.2015.08.025
Reference: YGAST 59985

To appear in: *Gastroenterology*
Accepted Date: 11 August 2015

Please cite this article as: Yu VZ, Wong VC-L, Dai W, Ko JM-Y, Lam AK-Y, Chan KW, Samant RS, Lung HL, Shuen WH, Law S, Chan YP, Lee NP-y, Tong DKH, Law TT, Lee VH-f, Lung ML, Nuclear Localization of DNAJB6 is Associated with Survival of Patients with Esophageal Cancer and Reduces AKT Signaling and Proliferation of Cancer Cells, *Gastroenterology* (2015), doi: 10.1053/j.gastro.2015.08.025.

Title:

Nuclear Localization of DNAJB6 is Associated with Survival of Patients with Esophageal Cancer and Reduces AKT Signaling and Proliferation of Cancer Cells

Short title:

Role of DNAJB6 in esophageal cancer

Authors:

Valen Zhuoyou Yu[1], Victor Chun-Lam Wong[1,7], Wei Dai[1], Josephine Mun-Yee Ko[1], Alfred King-Yin Lam[2], Kwok Wah Chan[3,6], Rajeev S. Samant[4], Hong Lok Lung[1,6], Wai Ho Shuen[1,8], Simon Law[5,6], Yuen Piu Chan[3], Nikki Pui-yue Lee[5,6], Daniel King Hung Tong[5], Tsz Ting Law[5], Victor Ho-fun Lee[1,6], Maria Li Lung[1,6]

[1]Department of Clinical Oncology, University of Hong Kong Li Ka Shing Faculty of Medicine, Pokfulam, Hong Kong, SAR

[2]Department of Cancer Molecular Pathology, Griffith Medical School and Menzies Health Institute Queensland, Griffith University, Gold Coast, Australia

[3]Department of Pathology, University of Hong Kong Li Ka Shing Faculty of Medicine, Hong Kong, SAR

[4]Department of Pathology, University of Alabama at Birmingham, Birmingham, AL, USA

[5]Department of Surgery, University of Hong Kong Li Ka Shing Faculty of Medicine, Pokfulam, Hong Kong, SAR

[6]Center for Cancer Research, University of Hong Kong Li Ka Shing Faculty of Medicine, Pokfulam, Hong Kong, SAR

[7]Current address: Cell Biology Program, Sloan-Kettering Institute for Cancer Research, New York, NY, USA

[8]Current address: Division of Medical Oncology, National Cancer Centre Singapore, Singapore

Grant support:

General Research Fund from Research Grants Council of Hong Kong Special Administrative Region, People's Republic of China (HKU 774411M) to MLL

Abbreviations:

ESCC: esophageal squamous cell carcinoma; EAC: esophageal adenocarcinoma; DNAJB6: DnaJ (Hsp40) homolog, subfamily B, member 6; HSP: heat shock protein; TMA: tissue microarray; IHC: immunohistochemical;

HR: hazard ratio; NLS: nuclear localization signal; NES: nuclear export signal; WT: wild type; NE: immortalized normal esophageal epithelial; VA: vector-alone; T308: threonine 308; S473: serine 473; fKO: functional knockout; PP2A: Protein phosphatase 2A; OA: okadaic acid; BiFC: bimolecular fluorescence complementation; NIR: near-infrared.

Correspondence:

Professor ML Lung

Room L6-43, 6/F, Laboratory Block, Faculty of Medicine Building, 21 Sassoon Road, Pokfulam, Hong Kong, SAR.

Tel: (852) 3917-9783

Fax: (852) 2816 6279

E-mail: mlilung@hku.hk

Disclosures:

The authors have nothing to disclose.

Author Contributions:

VZY, VCW, and MLL initiated study conception;

VZY and MLL designed experiments and interpreted data;

VZY performed experiments and drafted manuscript;

VZY, AKL, KWC, HLL, WHS, SL, YPC, NPL, DKHT, and TTL acquired data;

VCW, JMK, WD, AKL, RSS, HLL, and MLL revised manuscript;

VHL and MLL supervised study;

MLL obtained funding.

Abstract:

BACKGROUND & AIMS: The DnaJ (Hsp40) homolog, subfamily B, member 6 (DNAJB6) is part of a family of proteins that regulate chaperone activities. One of its isoforms, DNAJB6a, contains a nuclear localization signal and regulates β-catenin signaling during breast cancer development. We investigated the role of DNAJB6 in pathogenesis of esophageal squamous cell carcinoma (ESCC).

METHODS: We performed immunohistochemical analyses of primary ESCC samples and lymph node metastases from a cohort of 160 patients, who underwent esophagectomy with no pre-operative chemo-radiotherapy at Hong Kong Queen Mary Hospital. Data were collected on patient outcomes over a median time of 12.1±2.9 months. Retrospective survival association analyses were performed. Wild-type and mutant forms of DNAJB6a were overexpressed in cancer cell lines (KYSE510, KYSE 30TSI, KYSE140, and KYSE70TS), which were analyzed in proliferation and immunoblot assays, or injected subcutaneously into nude mice. Levels of DNAJB6 were knocked down in ESCC cell lines (KYSE450 and T.Tn), immortalized normal esophageal epithelial cell lines (NE3 and NE083), and other cells with short hairpin RNAs

or by genome engineering. Bimolecular fluorescence complementation was used to study interactions between proteins in living cells.

RESULTS: In primary ESCC samples, patients whose tumors had high nuclear levels of DNAJB6 had longer overall survival times (19.2±1.8 months; 95% confidence interval [CI], 15.6–22.8 months) than patients whose tumors had low nuclear levels of DNAJB6 (12.6±1.4 months; 95% CI, 9.8–15.4 months; *P*=.004, by log rank test). Based on Cox regression analysis, patients whose tumors had high nuclear levels of DNAJB6 had a lower risk of death than those with low levels (hazard ratio=0.562; 95% CI, 0.379–0.834; *P*=.004). Based on log rank analysis and Cox regression analysis, the combination of nuclear level of DNAJB6 and the presence of lymph node metastases at diagnosis could be used to stratify patients into groups with good or bad outcomes (*P*<.0005 for both analyses). There was a negative association between the nuclear level of DNAJB6 and the presence of lymph node metastases (*P*=.022; Pearson χ^2 test). Cancer cell lines that overexpressed DNAJB6a formed tumors more slowly in nude mice than control cells or cells that expressed a mutant form of DNAJB6a that did not localize to the nucleus. DNAJB6 knockdown in cancer cell lines promoted their growth as xenograft

tumors in mice. A motif of histidine, proline, and aspartic acid (HPD) in the J domain of DNAJB6a was required for its tumor suppressive effects and signaling via AKT1. Loss of DNAJB6a resulted in upregulation of AKT signaling in cancer cell lines and immortalized esophageal epithelial cells. Expression of a constitutively active form of AKT1 restored proliferation to tumor cells that overexpressed DNAJB6a, and DNAJB6a formed a complex with AKT1 in living cells. Expression of DNAJB6a reduced the sensitivity of ESCC to AKT inhibitors; the expression level of DNAJB6a affected AKT signaling in multiple cancer cell lines.

CONCLUSIONS: Nuclear localization of DNAJB6 is associated with longer survival times of patients with ESCC. DNAJB6a reduces AKT signaling, and DNAJB6 expression in cancer cells reduces their proliferation and growth of xenograft tumors in mice. DNAJB6a might be developed as biomarker for progression of ESCC.

KEYWORDS: prognostic marker; tissue microarray; signal transduction; tumor suppressor

INTRODUCTION

Esophageal carcinoma ranks as the eighth most frequent cancer worldwide, with an estimated 9% age-standardized incidence rate and 7.7% age-standardized mortality rate in 2012.[1] It is classified into two major histologic forms including esophageal squamous cell carcinoma (ESCC) and esophageal adenocarcinoma (EAC). EAC is more frequent in developed Western countries, while ESCC is the dominant histologic type in Asia including China and Hong Kong.[2]

The DNAJ/HSP40 family functions as co-chaperones, which modulate the activity and substrate specificity of chaperone proteins such as the HSP70 families. DNAJB6 is a member of the HSP40/DNAJ family. Two variants resulting from alternative splicing exist resulting in two protein isoforms, DNAJB6a and DNAJB6b.[3] Mutation of DNAJB6b has been detected and studied in limb-girdle muscular dystrophy.[4]

We reported the role of DNAJB6a in breast cancer is related to the regulation of the GSK3β/β-catenin pathway.[5-7] Herein, we studied the expression of DNAJB6 and correlates with the clinicopathological features of ESCC. The DNAJB6 nuclear isoform, DNAJB6a, was studied *in vivo* and *in vitro* to reveal its mechanisms in ESCC.

Materials and Methods details are in Supplementary Materials

Results

Nuclear DNAJB6 level is an independent prognostic marker for better survival

Kaplan-Meier survival analysis showed that high nuclear levels of DNAJB6 (DNAJB6_Hi) in primary tumors (n=160) were significantly correlated with better overall patient survival (median survival ± standard error: 19.2±1.8 months; 95% confidence interval [CI], 15.6-22.8 months) compared to low level (DNAJB6_Lo) (12.6±1.4 months; 95%CI, 9.8-15.4 months; *P*=.004 by Log-rank test, Figure 1A; Representative images shown in Supplementary Figure 1). Univariate Cox regression analysis showed that patients with high nuclear DNAJB6 levels have reduced risk of death (hazard ratio [HR] = 0.562, 95%CI, 0.379-0.834, *P*=.004), as compared to patients with low levels (HR=1). Multivariable Cox regression analysis confirmed nuclear DNAJB6 level is a predictor for overall survival (*P*=.025), independent from pathological stage, presence of lymph node metastases, and M stage (Table 1). These data suggest a general protective role of nuclear DNAJB6 in ESCC.

Combination of nuclear DNAJB6 level and status of lymph node metastasis at diagnosis could be used to stratify patients into two groups with differential risks of death

To further characterize possible associations behind the beneficial survival effect of nuclear DNAJB6 level, interaction tests with other prognostic clinical parameters were performed. Nuclear DNAJB6 level showed significant interaction with presence of lymph node metastasis (*P*<.05, Supplementary Table 1) and with M stage (*P*<.0005). Given the very limited sample size for M1 patients (n=12), we focused only on lymph node metastasis and further performed survival analyses regarding nuclear DNAJB6 level and presence of lymph node metastasis.

Kaplan-Meier survival analysis confirmed that the presence of lymph node metastases (LNM_+ve versus LNM_-ve) was significantly correlated with worse patient overall survival (n=99; 12.2±2.1 months; 95%CI, 8.1-16.3 months versus n=61; 23.1±4.1 months; 95%CI, 15.1-30.0 months, *P*=.003, Supplementary Figure 2). Indicated by the interaction test, we also confirmed that among patients without lymph node metastasis (n=61), nuclear DNAJB6 level still possesses prognostic value (*P*=.003, Supplementary Figure 3). We

further stratified the entire cohort into two groups according to their status of nuclear DNAJB6 level and lymph node metastasis. Interestingly, Kaplan-Meier survival analysis showed that patients with high nuclear DNAJB6 levels and no lymph node metastasis (DNAJB6_Hi/LNM_-ve) (n=33) displayed much better survival profiles (43.1±13.6 months; 95%CI, 16.4-69.7 months; *P*<.0005; Figure 1B), as compared to other patients either with low nuclear DNAJB6 level or with lymph node metastasis (DNAJB6_Lo or LNM_+ve, n=137; 13.15±1.5 months; 95%CI, 10.2-16.1 months). Univariate Cox regression analysis showed that patients with high nuclear DNAJB6 levels and no lymph node metastasis have significantly reduced risk of death (HR=0.359; 95%CI, 0.209-0.616; *P*<.0005), as compared to other patients (HR=1). This suggests that the combination of nuclear DNAJB6 level together with lymph node metastasis status at diagnosis serve as predictive indicators to stratify patients in two groups with very distinct prognostic features.

Nuclear DNAJB6 level in primary tumor is associated with presence of lymph node metastasis

We also found that patients with low nuclear DNAJB6 levels were more likely to have lymph node metastases, compared to patients with high levels

(*P*=.022, 2-sided by Pearson Chi-Square test, Supplementary Table 2).

However, in the 25 pairs of matched primary tumor/ lymph node metastases, 64% (16 pairs) showed comparable and 36% (9 pairs) showed differential nuclear DNAJB6 levels. Overall, nuclear DNAJB6 level is comparable between primary tumor and lymph node metastasis, suggesting loss of nuclear DNAJB6-mediated tumor-suppressive function occurs early before metastasis.

DNAJB6a encodes nuclear DNAJB6 and is downregulated in ESCC

There are two isoforms of DNAJB6, DNAJB6a and DNAJB6b, differing in their carboxy terminal sequences. A functional nuclear localization signal (NLS) was present in DNAJB6a[5] (Supplementary Figure 4). The presence of a functional nuclear export signal (NES) has not been reported for DNAJB6b. The subcellular localization of DNAJB6 in ESCC was examined by expressing fluorescence fusion proteins in two cell lines (Supplementary Figure**s** 5 and 6). Wild type (WT) DNAJB6a was mainly concentrated in the nucleus, while WT DNAJB6b diffuses throughout the cell. DNAJB6a ΔNLS loses the ability to reside in the nucleus completely, indicating a functional NLS in DNAJB6a in ESCC. The data also suggest a functional NES in DNAJB6b. These results

suggest that the nuclear DNAJB6 staining pattern in the tissue microarray (TMA) analysis mainly corresponds to the DNAJB6a isoform.

Expression of the *DNAJB6a* transcript was significantly downregulated in two sets of esophageal non-tumor/tumor tissue samples by hybridization–based oligonucleotide microarray analysis (GSE20347 and GSE29001) (probe 209015_s_at; *P*<.001 and =.030, respectively), but not the *DNAJB6b* transcript (probe 208810_at; *P*=.554 and .727, respectively) (Figure 1C). Expression of the *DNAJB6a* transcript was downregulated in 56.3% (9/16) and upregulated in 18.8% (3/16) of ESCC cell lines using an immortalized normal esophageal epithelial (NE) cell line, NE3, as a reference (Supplementary Figure 7). The expression of the *DNAJB6b* transcript does not show significant alteration.

DNAJB6a expression level affects tumorigenesis in mouse model and proliferation in a variant-specific and localization-dependent manner

DNAJB6a expressions were restored by over-expression in four tumorigenic cell lines with downregulated endogenous *DNAJB6a* expression, namely KYSE510/30TSI/140/70TS, and cells were injected subcutaneously into the mice and compared with cells expressing vector-alone (VA), diffusely localized *DNAJB6b*, and mislocalized *DNAJB6a* containing the deletion of the

NLS (*DNAJB6a* ΔNLS), as controls. Only the WT *DNAJB6a* over-expressing cells produce smaller tumors and display a 2- to 4-week lag period for tumor growth (Figure 2A, Supplementary Figures 8 and 9). Two cell lines, KYSE510 and KYSE30TSI, showing greater tumor-suppressive effects by *DNAJB6a* expression, were used for further functional and mechanistic analyses. Reversely, endogenous *DNAJB6a* expression knockdown in KYSE450 and T.Tn cell lines enhances *in vivo* tumor growth (Figures 2A, Supplementary Figure 10). These data collectively demonstrate that the expression of the nuclear DNAJB6 protein affects tumorigenicity *in vivo*, as observed with the TMA.

In vitro cell viability was assessed. WT *DNAJB6a*-over-expressing cells proliferate more slowly compared to VA, *DNAJB6a* ΔNLS, and *DNAJB6b*-over-expressing cells (Figure 2B, Supplementary Figure 11). *DNAJB6a* knockdown also results in increased proliferation (Figure 2B, Supplementary Figure 12). These data show the inhibitory effects of *DNAJB6a* on cell proliferation.

Flow cytometry study was performed to examine possible cell cycle regulation by *DNAJB6a*. After release from G1 synchronization, cells over-expressing *DNAJB6a* progress at a reduced rate towards G2 phase, as

compared to control cells (Figure 2C), while *DNAJB6a* knockdown promotes progression. As a control, cells over-expressing *DNAJB6a* go through mitosis at a comparable rate compared to control cells (Supplementary Figure 13).

DNAJB6a regulates AKT signaling in cancer cells

Consistent with the aforementioned results, the protein expression of cyclin E1 is downregulated in *DNAJB6a* over-expressing cells compared to VA cells both *in vivo* and *in vitro* (Figure 3A). *DNAJB6a* knockdown also upregulates cyclin E1 protein expression level *in vivo* and *in vitro* (Figure 3B). This is consistent with a previous finding that downregulation of cyclin E1 by microRNA reduced tumor growth and cell proliferation in ESCC.[8]

One of the major signaling pathways that regulates cyclin E1 protein expression is the AKT1/P27KIP1 pathway.[9-12] The phosphorylation status of threonine 308 (T308) and serine 473 (S473) of AKT1 was examined. Downregulation of phosphorylated AKT1, along with P27KIP1 upregulation, was observed in both *in vivo* and *in vitro DNAJB6a*-over-expressing cells (Figure 3A). Reduced *DNAJB6a* expression upregulates AKT1 phosphorylation and downregulates P27KIP1 *in vivo* and *in vitro* (Figure 3B). These data suggest that DNAJB6a acts through AKT1 to regulate P27KIP1,

leading to regulation of cyclin E1 protein expression.

To investigate the causality between cyclin E1 protein expression and AKT1 phosphorylation in ESCC, the effect of IGF-1, a well-known AKT1 pathway activator, on cells over-expressing *DNAJB6a* was investigated. The results show cyclin E1 protein expression is upregulated upon AKT1 activation by IGF-1, and AKT1 activation abolishes the down-regulation of cyclin E1 protein expression by *DNAJB6a* over-expression, indicating that cyclin E1 protein expression is downstream and a consequence of AKT1 activation in ESCC (Figure 3C). An AKT1 inhibitory assay was performed in *DNAJB6a*-knockdown cells. AKT inhibition abolishes the upregulation of cyclin E1 protein expression by *DNAJB6a* knockdown, further confirming a regulatory role of AKT1 on cyclin E1 protein expression (Figure 3D).

***DNAJB6a* regulates AKT signaling in immortalized normal cells**

TMA analysis showed no significant difference of nuclear DNAJB6 level related to early/late T-stage (*P*=.630, 2-sided by Pearson Chi-Square test, Supplementary Table 2), suggesting that loss of nuclear DNAJB6-mediated tumor-suppressive effect may occur early in ESCC development. We examined the role of *DNAJB6a* in precancerous cells using two NE cell lines

(NE3 and NE083) for *DNAJB6a* knockdown. *DNAJB6a* knockdown in NE cells increases AKT1 phosphorylation and upregulates the protein expression level of cyclin E1 (Figure 3E). AKT1 inhibition diminishes the upregulation of cyclin E1 protein expression by *DNAJB6a* knockdown (Figure 3F). This suggests that the DNAJB6a AKT1 regulatory effect generally applies under different circumstances.

Loss of DNAJB6a by variant-specific functional knockout (fKO) upregulates AKT signaling and enhances proliferation

Considering the possible non-specific targeting of mRNA variants by short hairpin RNA knockdown, the newly developed CRISPR-Cas9 genome engineering tool[13] was utilized to interfere with DNAJB6 protein expression by targeting a variant-specific exon leading to variant-specific sequence alterations (Supplementary Figure 4). Western blotting confirmed isoform-specific loss of DNAJB6 by variant-specific targeting oligo (Figure 4A). Consistent with the *DNAJB6a* knockdown results, DNAJB6a fKO upregulates AKT1 phosphorylation and cyclin E1 protein expression (Figure 4B) and enhances cell proliferation (Figure 4C, Supplementary Figure 14). The results further confirmed specific AKT regulation by the DNAJB6a isoform.

Proliferation and cell cycle regulation by DNAJB6a is AKT-dependent

To examine the causality between AKT regulation and proliferation inhibition by DNAJB6a, a myr-tagged constitutively active AKT1 construct (myrAKT) was introduced in *DNAJB6a* over-expressing cells to restore the down-regulated AKT activity. AKT activity rescue significantly eliminates the proliferation inhibitory effect (Figure 4D, Supplementary Figure 15), the cell cycle progression suppression (Figure 4E), and p27/cyclin E1 protein expression down-regulation (Figure 4F) in *DNAJB6a* over-expressing cells. The results strongly indicate that DNAJB6a acts through AKT activity regulation to inhibit proliferation and, thus, tumor suppression. Proliferation inhibition by DNAJB6a is AKT-dependent.

The HPD motif in the J domain is crucial for AKT signaling regulation and tumor-suppressive effects of *DNAJB6a*

DNAJ/HSP40 proteins rely heavily on the J domain containing a highly conserved tripeptide of histidine/proline/aspartic acid residues (HPD motif) for proper functioning. Therefore, a HPD motif dead *DNAJB6a* mutant, in which the tripeptide was changed to three alanines (AAA), was utilized to

characterize the molecular basis for *DNAJB6a* function in ESCC. Introduction of the mutant greatly abolishes the *in vivo* tumor-suppressive effect of WT *DNAJB6a*, as mutant over-expressing cells share similar growth kinetics with the control cells in mouse (Figure 5A, Supplementary Figure 16). Introduction of the mutant also abolishes the inhibitory effect on *in vitro* cell proliferation (Figure 5B, Supplementary Figure 17) and the regulation of both AKT1 phosphorylation and cyclin E1 protein expression (Figure 3A). These data demonstrate the critical role of the HPD motif in *DNAJB6a*-dependent tumor suppression in ESCC.

Protein phosphatase 2A (PP2A) activity is required for AKT signaling regulation of *DNAJB6a*

Inhibition of PP2A, a well-studied modulator of AKT1 phosphorylation,[14, 15] was applied to *DNAJB6a* over-expressing cells to investigate the involvement of PP2A phosphatase activity in the downregulation of AKT1 phosphorylation. Inhibition of PP2A phosphatase activity by treatment of a PP2A inhibitor okadaic acid (OA) greatly abolishes the downregulation of AKT1 phosphorylation by *DNAJB6a* over-expression in cell lines tested (Figure 5C), suggesting the requirement of PP2A phosphatase activity in AKT1 regulation

by *DNAJB6a*.

DNAJB6a complexes with AKT1 in living cells

To examine potential protein-protein interaction/complexing between DNAJB6a and AKT1 in living cells, a bimolecular fluorescence complementation (BiFC) live-cell imaging assay[16] was utilized. Remarkably, cells expressing the PAS-AKT1WT fusion protein together with the DNAJB6aWT-GAFm fusion proteins (PAS-AKT1WT/DNAJB6aWT-GAFm) showed significantly more NIR fluorescence signal-positive cells with distinct nuclear patterns (Figure 5D, Supplementary Figure 18), indicating an interaction/complexing between AKT1 and DNAJB6a. Consistent with the AKT1 regulation analysis, using the mutant *DNAJB6a* construct (*DNAJB6a-AAA*), cells co-expressing PAS-AKT1WT/DNAJB6aAAA-GAFm fusion proteins showed few NIR fluorescence signals. Introduction of a mutant AKT1 protein (K179M/T308A/S473A; MAA) fused to PAS domain also diminishes the protein complexing potential with DNAJB6a, when co-expressed with DNAJB6aWT-GAFm fusion protein in cells. These findings indicate that AKT1 and DNAJB6a can specifically form a complex in living cells.

DNAJB6a modulates cell sensitivity to AKT inhibition

Upon pharmaceutical AKT inhibition, ESCC cells over-expressing *DNAJB6a* became less sensitive to inhibition and showed a significantly higher viability, while in contrast, cells with *DNAJB6a*-knockdown showed significantly higher sensitivity and lower viability, as compared to control cells, respectively (Figure 6A). As a control, cells did not show alteration of sensitivity to inhibition of the mitogen-activated protein kinase. These results suggest that modulation of AKT1 phosphorylation by DNAJB6a confers opposing functional consequences to the survival of the cells upon inhibition of the AKT signaling.

DNAJB6a modulates AKT signaling in other type of cancer cells

The possibility that *DNAJB6a* acts as a more general AKT regulator in various cell lines was tested for various cancer/tissue types by *DNAJB6a* over-expression or knockdown. Interestingly, *DNAJB6a* regulates AKT signaling only in a subset of cell lines, including A549, HepG2, HONE1, and NP460 cells, but not in others (Figure 6B). Therefore, these data suggest that DNAJB6a may act as a general AKT regulator in a tissue-specific manner.

We further examined the expression levels of *DNAJB6a* transcripts in

other cancers using publicly available microarray data. Interestingly *DNAJB6a* expression is down-regulated in EAC, another major subtype of esophageal cancer. We did not observe significant down-regulation of *DNAJB6a* transcripts in other cancer types (Supplementary Figure 19).

Over-expression of *DNAJB6a* does not suppress lung colonization in a distant metastasis mouse model

To explore the functional effect of DNAJB6a on metastasis, a tail-vein metastasis mouse model was utilized. *In vivo* bioluminescent imaging showed that cells over-expressing *DNAJB6a* colonize the lungs of the mice at a comparable rate as compared to cells over-expressing VA (Supplementary Figures 20 and 21). The survival data also showed consistency with the imaging result. Mice injected with cells over-expressing *DNAJB6a* share similar survival dynamics (*P*=.496 by Log-rank test, Supplementary Figure 22). These data indicate that expression of *DNAJB6a* elicits no inhibitory effect on metastasis, as opposed to that on primary tumor.

Discussion

This study provides the first evidence of a tumor-suppressive role of

DNAJB6 in ESCC. The TMA analysis indicates that nuclear DNAJB6 is an independent indicator for better overall survival in Hong Kong ESCC patients. We also found that there is significant interaction between nuclear DNAJB6 level and presence of lymph node metastasis. Furthermore, combining the status of nuclear DNAJB6 level and lymph node metastasis at diagnosis could be used to stratify ESCC patients into two groups with significantly differential risks of death and outcomes.

We showed that DNAJB6a localizes to the nucleus due to the existence of a functional NLS at the C-terminal end and DNAJB6b diffuses throughout the cell in ESCC. Therefore, the observed nuclear DNAJB6 staining pattern in tumor specimens corresponds mostly to the DNAJB6a isoform. Cell line-based models showed that the tumor-suppressive effect is isoform-specific. Consistent with the TMA result, only over-expression of nucleus-localized WT *DNAJB6a* induces *in vivo* tumor suppression and *in vitro* proliferation inhibition. This is consistent with our previous findings that *DNAJB6a* suppresses tumor growth in breast cancer.[5, 7] By introducing a constitutively active AKT1 construct to compensate for the down-regulated AKT1 activity in *DNAJB6a* over-expressing cells, we showed that the proliferation inhibition induced by DNAJB6a is AKT1-dependent, indicating that DNAJB6a acts through AKT1

regulation to inhibit proliferation and, thus, tumor suppression. In our previous studies, *DNAJB6a* was reported to regulate the Wnt/β-Catenin signaling.[6, 7] This indicates that *DNAJB6a* plays a tissue-specific role.

The current study revealed a novel AKT signaling regulation by a member of the DNAJ/HSP40 family in cancer. As a major oncogenic player, continuous activation of AKT signaling usually results from aberrant upstream signals that phosphorylate AKT1 at T308 and S473.[17] Phosphorylation at both sites is strictly controlled by interactions with kinases and phosphatases.[18] The AKT signaling pathway is highly activated in ESCC through over-expression, amplification, and mutation events.[19] We showed that the DNAJB6a regulates phosphorylation of AKT1 and the dependent downstream effects and a functioning protein phosphatase PP2A is needed for such regulation (Figure 6C). We also showed AKT signaling regulation by *DNAJB6a* expression in normal immortalized esophageal epithelial cells, indicating that loss of *DNAJB6a* in precancerous tissues may elicit oncogenic features.

Mechanistically, the analyses using mutant *DNAJB6a* in functional and molecular analysis showed for the first time in ESCC that the tumor suppression of *DNAJB6a* essentially relies on the HPD motif in the J-domain. Members of the DNAJ/HSP40 family bind and stimulate the ATP-hydrolysis

activity of HSP70 through the highly conserved HPD motif in J-domain.[20-22] Utilizing a NIR fluorescent protein-based BiFC imaging assay, we showed that DNAJB6a and AKT1 specifically form complexes in living cells in a HPD motif-dependent manner. We also confirmed that DNAJB6a interacts with HSP70 using the co-immunoprecipitation assay in ESCC cells (Supplementary Figure 23). In our previous study, we showed that DNAJB6a interacts with the PP2A catalytic subunit in cancer cells.[7] HSP70 has been implicated to interact with PP2A.[23, 24] Therefore, we propose a mechanistic hypothesis that DNAJB6a complexes with HSP70/PP2A/AKT1 in the nucleus and promotes dephosphorylation of AKT1 by PP2A.

DNAJB6a expression also modifies cellular sensitivity to AKT inhibition by a small molecule inhibitor. Increasing *DNAJB6a* expression level leads to downregulated AKT signaling but also decreased sensitivity to AKT inhibition, and vice versa, suggesting that ESCC cells adapt to elevated oncogenic signaling and gain addiction. This suggests that AKT hypoactivation by *DNAJB6a* and AKT inhibition by a chemical inhibitor does not work synergistically, which may provide insight into molecular targeted therapy focusing on oncogene addiction.

In order to examine whether the effect on AKT signaling regulation of

DNAJB6a is ESCC-specific or represents a more general phenomenon, several cell lines from other cancer types or immortalized normal cells were studied. *DNAJB6a* expression modulation regulates AKT1 phosphorylation in four of the eight cell lines tested, indicating a tissue-specific role. This is akin to the reported tissue-specific expression of various PP2A regulatory subunits[25]. Intriguingly, in a recent study by Zhang *et al.*, *DNAJB6* expression was found to be oncogenic and to promote invasion in colorectal cancer in SW480,[26] consistent with our data for a tissue-specific role. However, we did not observe significant down-regulation of *DNAJB6a* transcripts in clinical samples of other cancer types. This may be due to the complexities of different cancers in which *DNAJB6a* plays different roles. Further studies on DNAJB6a protein expression levels and functional studies are needed to fully assess its functional impact in these cancer types. Interestingly, *DNAJB6a* shows significant down-regulation in EAC clinical samples, similar to ESCC, indicating that generally in esophageal cancer *DNAJB6a* likely plays an important tumor-suppressive role. Detailed functional and molecular assays of *DNAJB6a* in EAC are warranted.

The mouse model indicated that *DNAJB6a* does not possess suppressive effects in distant metastasis. A previous study indicated that AKT1 activated by

the chemokine receptor CXCR4 in oral squamous cell carcinoma promoted lymph node metastasis, but not distant metastasis[27]. These data suggest a differential role of DNAJB6a, likely involving AKT-regulated signaling in primary tumor growth, lymph node metastasis, and distant metastasis.

The current study is, however, limited by several factors. Firstly, patients enrolled in the study were from a single institute. A larger multi-institutional validation cohort is needed to verify the clinical utility of using the DNAJB6 level as predictive indicators. Secondly, due to the limited sample size, subgroup analysis lacked substantial statistical power. Furthermore, there is currently no available mouse sporadic ESCC model for detailed examination of functional and molecular properties of DNAJB6.

This study shows that nuclear DNAJB6 is a tumor suppressor in ESCC and plays a critical role in the development of primary ESCC. This study also provides new insights into the regulation of AKT signaling and suggests the potential for the usefulness of DNAJB6 as a prognostic and therapeutic biomarker for ESCC.

Acknowledgements

We acknowledge the Research Grants Council of Hong Kong for funding support (HKU 774411M to MLL). We thank Griffith University and staff in Cancer Molecular Pathology team for funding and setting up one of the TMAs. We thank Prof. Masaki Inagaki (Aichi Cancer Center Research Institute, Japan) for providing the pRK5-Myc-*DNAJB6b* plasmid. We acknowledge DSMZ (German Collection of Microorganisms and Cell Culture) for the KYSE cell lines. We thank Prof. Gopesh Srivastava, Dr. Annie Lai Man Cheung, and Prof. George Tsao for cell lines. We acknowledge the University of Hong Kong Faculty of Medicine Core Facility for providing facilities for flow cytometry, confocal microscopy imaging, and live animal imaging.

Figure Legends

Figure 1. Nuclear DNAJB6 expression as a good prognostic marker. (A) Kaplan-Meier analysis showed that nuclear DNAJB6 level was a prognostic marker. (B) Kaplan-Meier analysis showed that nuclear DNAJB6 level together with presence of lymph node metastasis could be used to further stratify patients into different groups with distinct survival outcomes. (C) *DNAJB6a* transcript was significantly downregulated in two sets of ESCC non-tumor/tumor specimens.

Figure 2. Suppression of tumor growth and cell proliferation of *DNAJB6a*. (A) Summary of *in vivo* tumor growth of *DNAJB6*-over-expressing or *DNAJB6a*-knockdown cells in subcutaneous tumorigenicity mouse models. For individual growth curves and protein expressions see Figure 3B and Supplementary Figures 7-9. Time points presented: week 4 for KYSE510, KYSE30TSI, and KYSE140; week 3 for KYSE70TS; week 5 for KYSE450 and T.Tn. (B) Summary of *in vitro* proliferation. For individual growth curves see Supplementary Figures 10 and 11. Time points presented: day 5 for KYSE510, KYSE450, and T.Tn; day 6 for KYSE30TSI. (C) Cell cycle progression after release from G1 synchronization. Recovery time: 18 hours for KYSE510; 30 hours for KYSE30TSI; 23 hours for KYSE450; 20 hours for T.Tn. $^{\#}$: adjusted

P<.1; ##: adjusted *P*<.05; ###: adjusted *P*<.01; ####: adjusted *P*<.001; n.s.: adjusted *P*>.1. ***: *P*<.001; ctrl: non-targeting control oligo.

Figure 3. AKT signaling regulation of *DNAJB6a*. (A) Western blotting shows downregulated cyclin E1 protein expression and AKT1 phosphorylations with upregulated p27KIP1 protein expression in *DNAB6a*-over-expressing cells both *in vivo* and *in vitro*. Introduction of HPD motif dead mutant (AAA) greatly abolished the regulation of AKT signaling. (B) Western blotting showed upregulated cyclin E1 protein expression and AKT1 phosphorylations with downregulated p27KIP1 protein expression in *DNAJB6a*-knockdown cells both *in vivo* and *in vitro*. (C) Western blotting showed that cyclin E1 protein expression is upregulated after AKT1 activation by IGF-1, and that AKT1 activation greatly abolishes the downregulation of cyclin E1 protein expression by *DNAJB6a* over-expression. (D) Western blotting revealed that AKT inhibition (AKTi) diminishes the upregulation of cyclin E1 protein expression in *DNAJB6a*-knockdown cells. (E) Western blotting showed upregulated cyclin E1 protein expression and AKT1 phosphorylations with downregulated p27KIP1 protein expression in *DNAB6a*-knockdown NE cells. (F) Western blotting shows that AKT inhibition diminishes the upregulation of cyclin E1 protein expression in *DNAJB6a*-knockdown NE cells. VA: vector-alone; Da:

DNAJB6a; ctrl: non-targeting control oligo; shDa: DNAJB6a knockdown.

Figure 4. Isoform-specific DNAJB6a fKO assay and AKT activity rescue assay. (A) Western blotting confirms isoform-specific loss of DNAJB6a/b by variant-specific targeting oligos. (B) Western blotting shows DNAJB6a fKO upregulates AKT signaling. (C) Summary of *in vitro* proliferation of DNAJB6a fKO cells. For individual cell line growth curves see Supplementary Figure 13. Time points presented: day 5 for KYSE450 and T.Tn. (D) Summary of *in vitro* proliferation of cells expressing constitutively active AKT1 construct. For individual cell line growth curves see Supplementary Figure 14. Time points presented: day 5 for KYSE510 and day 7 for KYSE30TSI. (E) Cell cycle progression after release from G1 synchronization of AKT activity rescued cells. Recovery time: 20 hours for KYSE510; 28 hours for KYSE30TSI; (F) Western blotting shows that the molecular changes induced by DNAJB6a expression are reversed by AKT activity rescue. $^{\#}$: adjusted P<.1; $^{\#\#}$: adjusted P<.05; $^{\#\#\#}$: adjusted P<.01; ctrl: non-targeting control oligo; sgRNA1 and sgRNA2: sgRNA specifically targets *DNAJB6a*. myrAKT: myr-tagged constitutively active AKT1 construct; VA: vector-alone; Da: DNAJB6a expression; Da+: DNAJB6a expression with constitutively active AKT1 expression.

Figure 5. Mechanistic analysis of AKT signaling regulation of *DNAJB6a*. (A) Summary of *in vivo* tumor growth of WT and mutant *DNAJB6a* (AAA) over-expressing cells in subcutaneous mouse models. For individual cell line growth curves and protein expressions see Figure 3A and Supplementary Figure 15. Time points presented: week 4 for KYSE510 and week 5 for KYSE30TSI. (B) Summary of *in vitro* proliferation. For individual cell line growth curves see Supplementary Figure 16. Time points presented: day 5 for KYSE510 and day 7 for KYSE30TSI. The *in vivo* tumor growth and *in vitro* proliferation profiles of VA and WT *DNAJB6a* over-expressing cells of KYSE510 and KYSE30TSI in (A) and (B) were duplicated from Figure 2A and 2B, respectively, as these data were generated from the same batches of samples. (C) PP2A inhibition by OA treatment greatly abolished the regulation of AKT1 phosphorylation by DNAJB6a over-expression. (D) Summary of NIR-positive cell percentages of images from cells expressing different pairs of fusion proteins. Cells expressing the PAS-AKT1WT fusion protein with the DNAJB6aWT-GAFm fusion protein (AKT1WT/DNAJB6aWT) showed significantly more NIR fluorescence signal- positive cells, as compared to cells expressing mutants of either protein (AKT1MAA/DNAJB6aWT and AKT1WT/DNAJB6aAAA). $^{\#\#}$: adjusted $P<.05$; $^{\#\#\#}$: adjusted $P<.01$; $^{\#\#\#\#}$: adjusted

P<.001; n.s.: adjusted *P*>.1.

Figure 6. *DNAJB6a* modulation of cellular sensitivity to AKT inhibition in ESCC and AKT signaling regulation in other types of cells. (A) Summary of *in vitro* cell viability test of cells with *DNAJB6a* over-expression or *DNAJB6a* knockdown showing cellular sensitivity to AKT inhibition (AKTi) and MEK inhibition (MEKi). ctrl: DMSO treatment. **: *P*<.01; n.s.: not statically significant. (B) Western blotting showed that modulation of DNAJB6a expression regulates AKT signaling only in a subgroup of cell lines tested (Responsive versus Non-responsive). VA: vector-alone; Da: DNAJB6a; ctrl: non-targeting control oligo; shDa: DNAJB6a knockdown. (C) Proposed model illustrating the mechanism of tumor suppression of *DNJAB6a* in ESCC.

Table Legend

Table 1. Univariate and multivariable survival analyses of clinical parameters and nuclear expression of DNAJB6 protein. CI: Confidence interval; HR: hazard ratio. HR larger than 1 indicates poor prognostic effect and vice versa. [a]: HR=0.621 indicates patients with high DNAJB6 levels have better prognosis than patients with low levels; [b]: HR=2.019 indicates late stage (III/IV) patients have worse prognosis than early stage (I/II) patients.

References

1. Ferlay J, Soerjomataram I, Dikshit R, et al. Cancer incidence and mortality worldwide: sources, methods and major patterns in GLOBOCAN 2012. Int J Cancer 2015;136:E359-86.
2. Zhang HZ, Jin GF, Shen HB. Epidemiologic differences in esophageal cancer between Asian and Western populations. Chin J Cancer 2012;31:281-6.
3. Hanai R, Mashima K. Characterization of two isoforms of a human DnaJ homologue, HSJ2. Mol Biol Rep 2003;30:149-53.
4. **Sarparanta J**, **Jonson PH**, **Golzio C**, et al. Mutations affecting the cytoplasmic functions of the co-chaperone DNAJB6 cause limb-girdle muscular dystrophy. Nat Genet 2012;44:450-5, S1-2.
5. Mitra A, Fillmore RA, Metge BJ, et al. Large isoform of MRJ (DNAJB6) reduces malignant activity of breast cancer. Breast Cancer Res 2008;10:R22.
6. Mitra A, Menezes ME, Shevde LA, et al. DNAJB6 induces degradation of beta-catenin and causes partial reversal of mesenchymal phenotype. J Biol Chem 2010;285:24686-94.
7. Mitra A, Menezes ME, Pannell LK, et al. DNAJB6 chaperones PP2A

mediated dephosphorylation of GSK3beta to downregulate beta-catenin transcription target, osteopontin. Oncogene 2012;31:4472-83.

8. Ding DP, Chen ZL, Zhao XH, et al. miR-29c induces cell cycle arrest in esophageal squamous cell carcinoma by modulating cyclin E expression. Carcinogenesis 2011;32:1025-32.

9. Liang J, Zubovitz J, Petrocelli T, et al. PKB/Akt phosphorylates p27, impairs nuclear import of p27 and opposes p27-mediated G1 arrest. Nat Med 2002;8:1153-60.

10. Viglietto G, Motti ML, Bruni P, et al. Cytoplasmic relocalization and inhibition of the cyclin-dependent kinase inhibitor p27(Kip1) by PKB/Akt-mediated phosphorylation in breast cancer. Nat Med 2002;8:1136-44.

11. Aggarwal BB, Banerjee S, Bharadwaj U, et al. Curcumin induces the degradation of cyclin E expression through ubiquitin-dependent pathway and up-regulates cyclin-dependent kinase inhibitors p21 and p27 in multiple human tumor cell lines. Biochem Pharmacol 2007;73:1024-32.

12. Bloom J, Pagano M. Deregulated degradation of the cdk inhibitor p27 and malignant transformation. Semin Cancer Biol 2003;13:41-7.

13. Hsu PD, Lander ES, Zhang F. Development and applications of CRISPR-Cas9 for genome engineering. Cell 2014;157:1262-78.

14. Andjelkovic M, Jakubowicz T, Cron P, et al. Activation and phosphorylation of a pleckstrin homology domain containing protein kinase (RAC-PK/PKB) promoted by serum and protein phosphatase inhibitors. Proc Natl Acad Sci U S A 1996;93:5699-704.

15. Ugi S, Imamura T, Maegawa H, et al. Protein phosphatase 2A negatively regulates insulin's metabolic signaling pathway by inhibiting Akt (protein kinase B) activity in 3T3-L1 adipocytes. Mol Cell Biol 2004;24:8778-89.

16. Filonov GS, Verkhusha VV. A near-infrared BiFC reporter for in vivo imaging of protein-protein interactions. Chem Biol 2013;20:1078-86.

17. Vivanco I, Sawyers CL. The phosphatidylinositol 3-Kinase AKT pathway in human cancer. Nat Rev Cancer 2002;2:489-501.

18. Scheid MP, Woodgett JR. Unravelling the activation mechanisms of protein kinase B/Akt. FEBS Lett 2003;546:108-12.

19. **Lin DC**, **Hao JJ**, **Nagata Y**, et al. Genomic and molecular characterization of esophageal squamous cell carcinoma. Nat Genet 2014.

20. Wall D, Zylicz M, Georgopoulos C. The NH2-terminal 108 amino acids of the Escherichia coli DnaJ protein stimulate the ATPase activity of DnaK and are sufficient for lambda replication. J Biol Chem 1994;269:5446-51.

21. Tsai J, Douglas MG. A conserved HPD sequence of the J-domain is necessary for YDJ1 stimulation of Hsp70 ATPase activity at a site distinct from substrate binding. J Biol Chem 1996;271:9347-54.

22. Hennessy F, Cheetham ME, Dirr HW, et al. Analysis of the levels of conservation of the J domain among the various types of DnaJ-like proteins. Cell Stress Chaperones 2000;5:347-58.

23. Polanowska-Grabowska R, Simon CG, Jr., Falchetto R, et al. Platelet adhesion to collagen under flow causes dissociation of a phosphoprotein complex of heat-shock proteins and protein phosphatase 1. Blood 1997;90:1516-26.

24. Whalen KA, de Jesus R, Kean JA, et al. Genetic analysis of the polyomavirus DnaJ domain. J Virol 2005;79:9982-90.

25. McCright B, Virshup DM. Identification of a new family of protein phosphatase 2A regulatory subunits. J Biol Chem 1995;270:26123-8.

26. Zhang TT, Jiang YY, Shang L, et al. Overexpression of DNAJB6

promotes colorectal cancer cell invasion through an IQGAP1/ERK-dependent signaling pathway. Mol Carcinog 2014.

27. Uchida D, Begum NM, Tomizuka Y, et al. Acquisition of lymph node, but not distant metastatic potentials, by the overexpression of CXCR4 in human oral squamous cell carcinoma. Lab Invest 2004;84:1538-46.

Author names in bold designate shared co-first authors.

Univariate survival analyses

	Median (Month)	95% CI	*p*-value
Nuclear DNAJB6 level			**.004**
High expression	19.2	15.6-23.0	
Low expression	12.6	9.8-15.4	
Pathological stage			**<.0005**
I & II	24.4	12.0-36.8	
III & IV	11.3	9.1-13.4	
T stage			.174
T1 & 2	24.3	13.7-34.9	
T3 & 4	14.1	10.7-17.4	
Lymph node metastasis			**.003**
Positive	12.2	8.1-16.3	
Negative	23.1	15.1-31.0	
M stage			**.025**
M0	16.0	13.3-18.6	
M1/1a/1b	6.3	5.7-6.8	
Grade			.542
G1 (Well-differentiated)	13.2	6.7-20.0	
G2 (Moderately differentiated)	14.3	10.6-18.0	
G3 (Poorly differentiated)	19.6	15.4-23.8	

Multivariate survival analyses

	HR	95% CI	*p*-value
Nuclear DNAJB6 level	.621[a]	0.409-0.943	**.025**
Pathological stage	2.019[b]	1.105-3.689	**.022**
Lymph node metastasis	.958	0.537-1.710	.886
M stage	1.340	0.676-2.657	.402

A

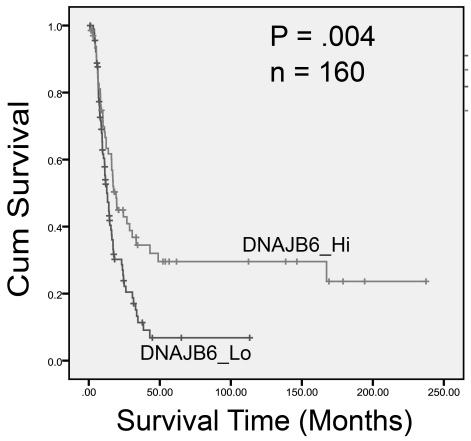

B

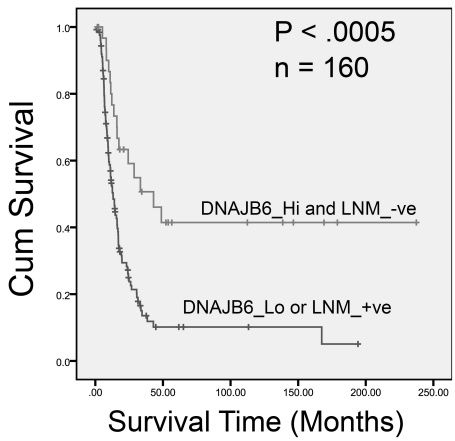

C

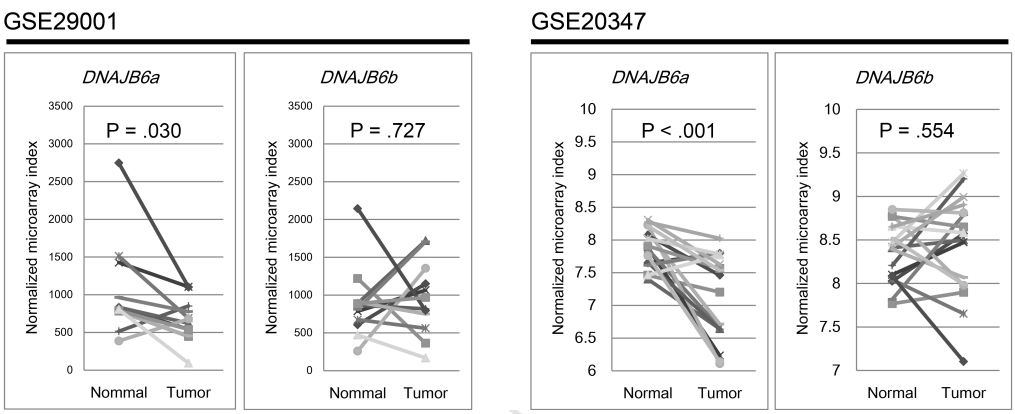

A

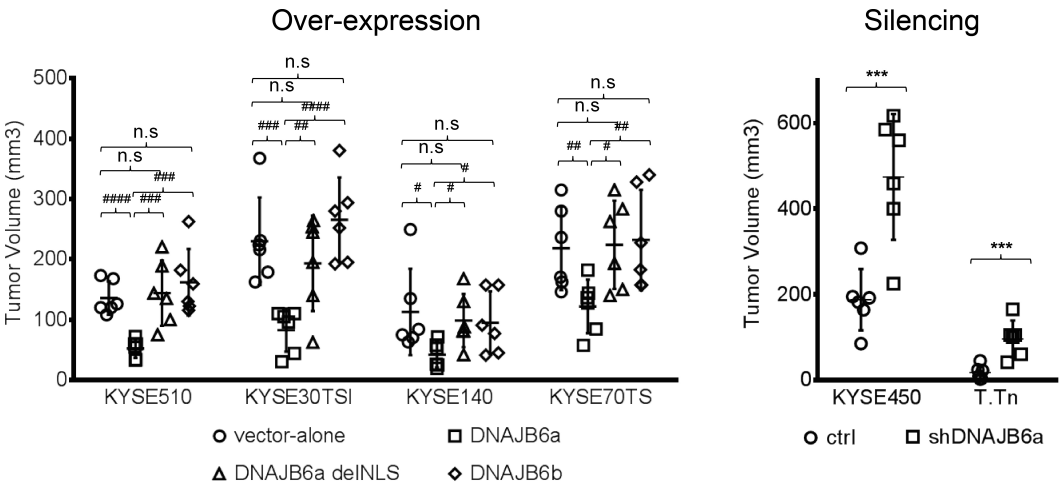
Over-expression
Silencing
Tumor Volume (mm3)
KYSE510
KYSE30TSI
KYSE140
KYSE70TS
KYSE450
T.Tn
vector-alone
DNAJB6a
DNAJB6a delNLS
DNAJB6b
ctrl
shDNAJB6a

B

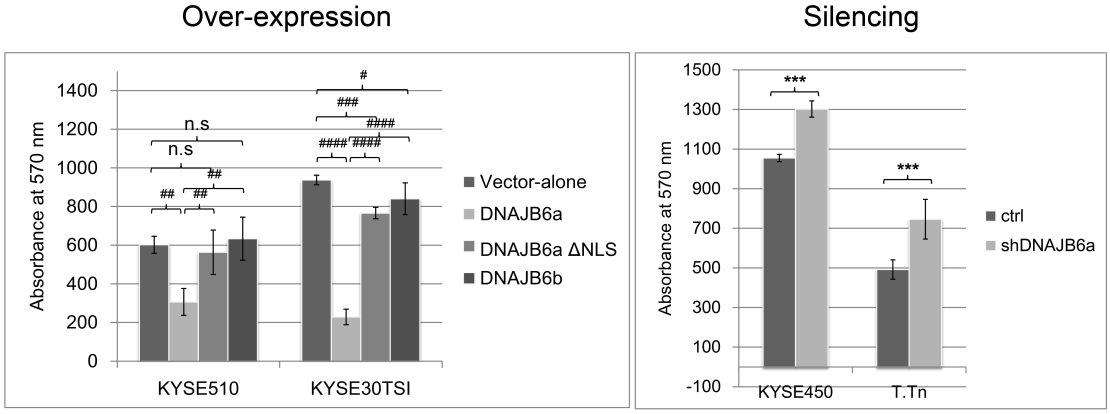
Over-expression
Silencing
Absorbance at 570 nm
KYSE510
KYSE30TSI
KYSE450
T.Tn
Vector-alone
DNAJB6a
DNAJB6a ΔNLS
DNAJB6b
ctrl
shDNAJB6a

C

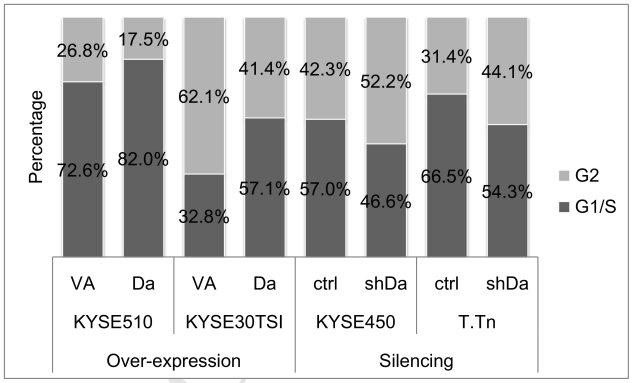
Percentage
26.8%
72.6%
17.5%
82.0%
62.1%
32.8%
41.4%
57.1%
42.3%
57.0%
52.2%
46.6%
31.4%
66.5%
44.1%
54.3%
G2
G1/S
VA
Da
VA
Da
ctrl
shDa
ctrl
shDa
KYSE510
KYSE30TSI
KYSE450
T.Tn
Over-expression
Silencing

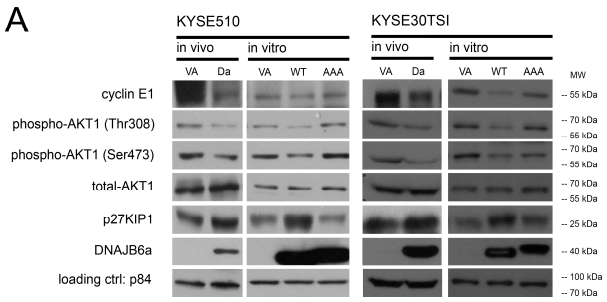

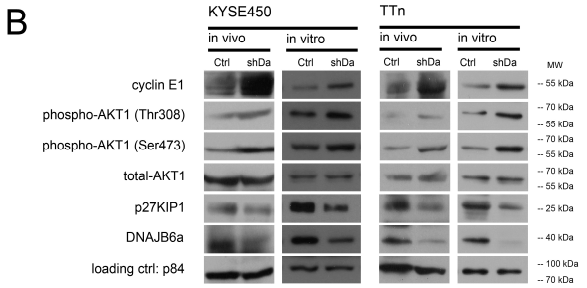

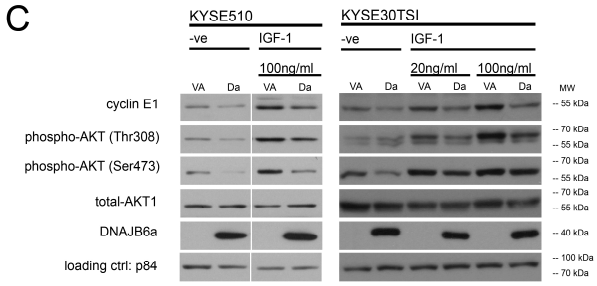

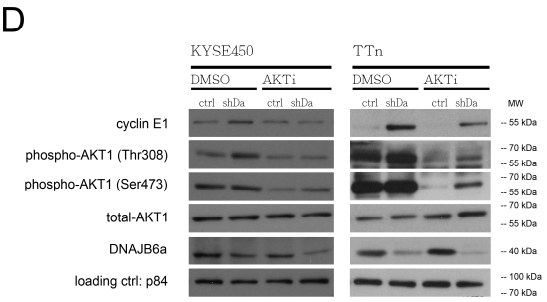

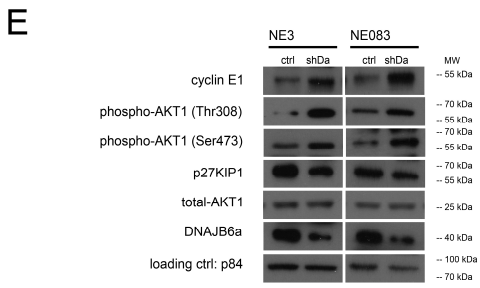

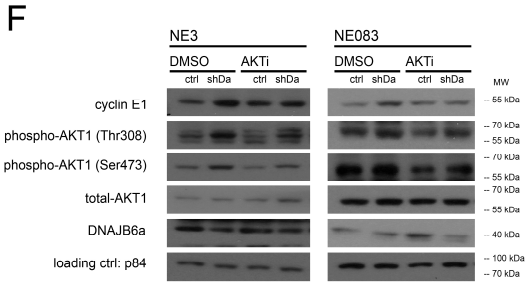

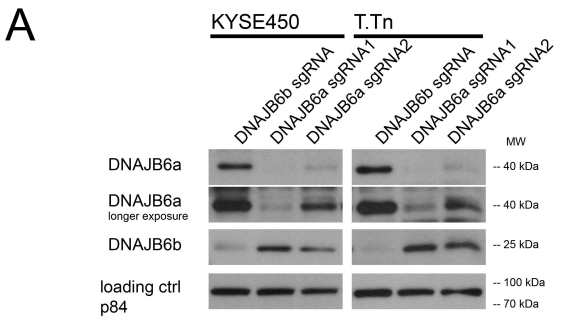
A
KYSE450
T.Tn
DNAJB6b sgRNA
DNAJB6a sgRNA1
DNAJB6a sgRNA2
DNAJB6b sgRNA
DNAJB6a sgRNA1
DNAJB6a sgRNA2
MW
DNAJB6a
DNAJB6a
longer exposure
DNAJB6b
loading ctrl
p84
-- 40 kDa
-- 40 kDa
-- 25 kDa
-- 100 kDa
-- 70 kDa

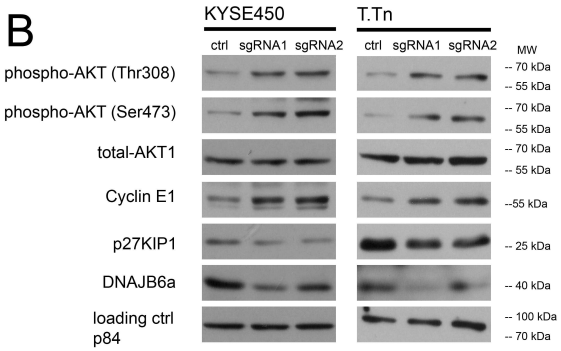
B
KYSE450
T.Tn
ctrl
sgRNA1
sgRNA2
ctrl
sgRNA1
sgRNA2
MW
phospho-AKT (Thr308)
phospho-AKT (Ser473)
total-AKT1
Cyclin E1
p27KIP1
DNAJB6a
loading ctrl
p84
-- 70 kDa
-- 55 kDa
-- 70 kDa
-- 55 kDa
-- 70 kDa
-- 55 kDa
--55 kDa
-- 25 kDa
-- 40 kDa
-- 100 kDa
-- 70 kDa

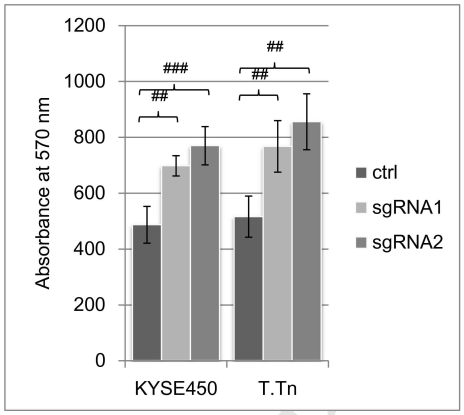
C
Absorbance at 570 nm
1200
1000
800
600
400
200
0
###
##
##
##
KYSE450
T.Tn
ctrl
sgRNA1
sgRNA2

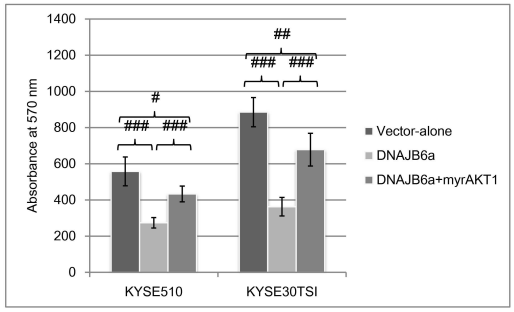
D
Absorbance at 570 nm
1400
1200
1000
800
600
400
200
0
#
###
###
##
###
###
KYSE510
KYSE30TSI
Vector-alone
DNAJB6a
DNAJB6a+myrAKT1

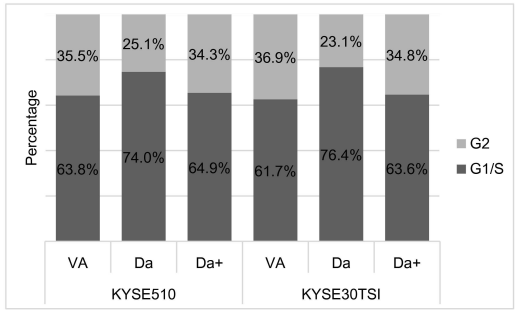
E
Percentage
35.5%
63.8%
25.1%
74.0%
34.3%
64.9%
36.9%
61.7%
23.1%
76.4%
34.8%
63.6%
VA
Da
Da+
VA
Da
Da+
KYSE510
KYSE30TSI
G2
G1/S

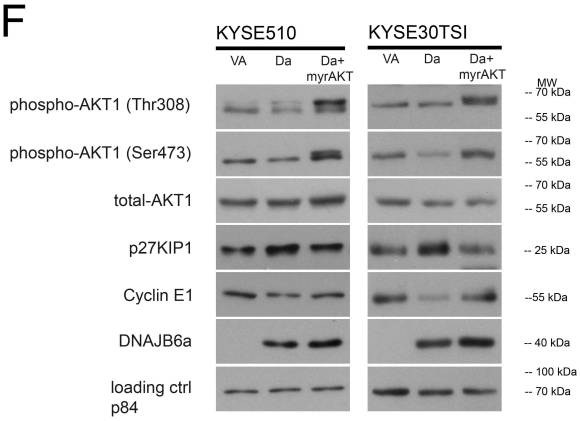
F
KYSE510
KYSE30TSI
VA
Da
Da+
myrAKT
VA
Da
Da+
myrAKT
MW
phospho-AKT1 (Thr308)
phospho-AKT1 (Ser473)
total-AKT1
p27KIP1
Cyclin E1
DNAJB6a
loading ctrl
p84
-- 70 kDa
-- 55 kDa
-- 70 kDa
-- 55 kDa
-- 70 kDa
-- 55 kDa
-- 25 kDa
--55 kDa
-- 40 kDa
-- 100 kDa
-- 70 kDa

A

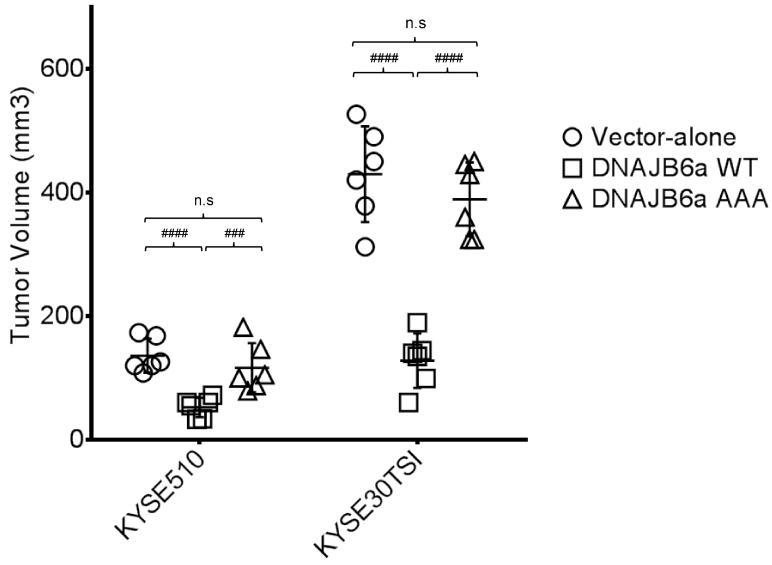
Tumor Volume (mm3)
600
400
200
0
n.s
####
###
n.s
####
####
KYSE510
KYSE30TSI
Vector-alone
DNAJB6a WT
DNAJB6a AAA

B

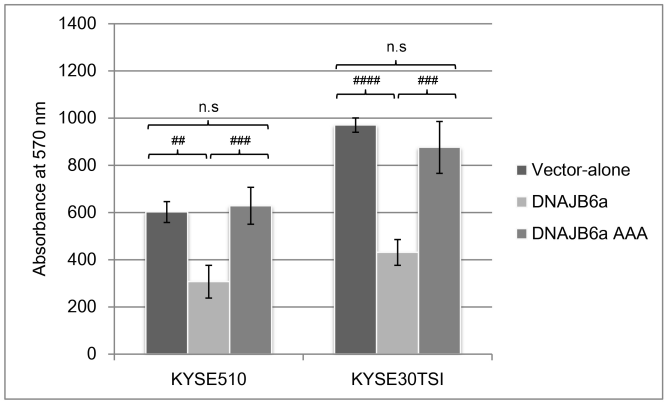
Absorbance at 570 nm
1400
1200
1000
800
600
400
200
0
n.s
##
###
n.s
####
###
KYSE510
KYSE30TSI
Vector-alone
DNAJB6a
DNAJB6a AAA

C

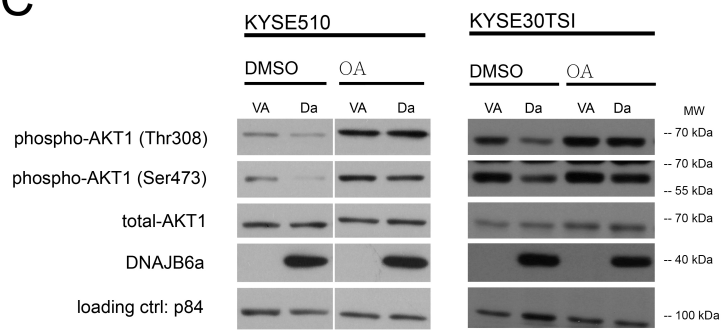
KYSE510
KYSE30TSI
DMSO
OA
DMSO
OA
VA
Da
VA
Da
VA
Da
VA
Da
MW
phospho-AKT1 (Thr308)
phospho-AKT1 (Ser473)
total-AKT1
DNAJB6a
loading ctrl: p84
-- 70 kDa
-- 70 kDa
-- 55 kDa
-- 70 kDa
-- 40 kDa
-- 100 kDa

D

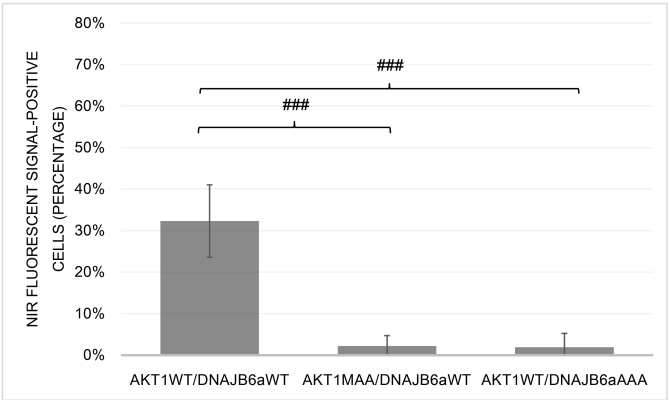
NIR FLUORESCENT SIGNAL-POSITIVE CELLS (PERCENTAGE)
80%
70%
60%
50%
40%
30%
20%
10%
0%
###
###
AKT1WT/DNAJB6aWT
AKT1MAA/DNAJB6aWT
AKT1WT/DNAJB6aAAA

A

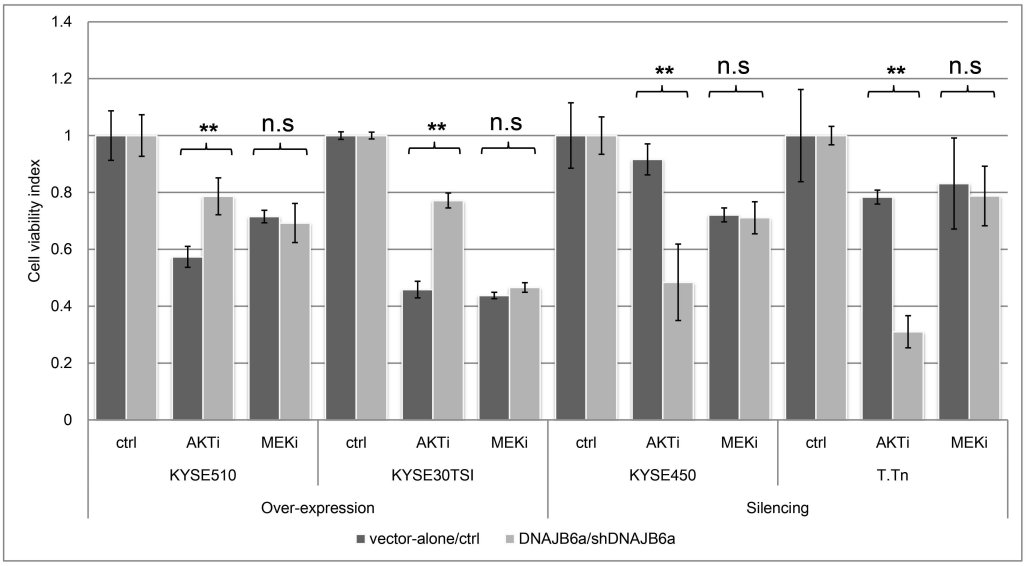
Cell viability index
1.4
1.2
1
0.8
0.6
0.4
0.2
0
**
n.s
ctrl
AKTi
MEKi
KYSE510
KYSE30TSI
KYSE450
T.Tn
Over-expression
Silencing
vector-alone/ctrl
DNAJB6a/shDNAJB6a

B

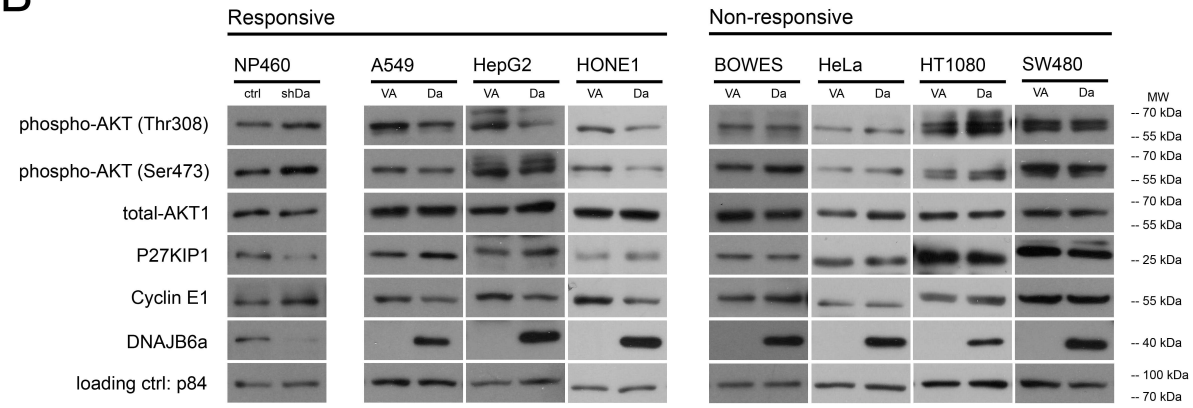
Responsive
Non-responsive
NP460
A549
HepG2
HONE1
BOWES
HeLa
HT1080
SW480
ctrl
shDa
VA
Da
MW
phospho-AKT (Thr308)
phospho-AKT (Ser473)
total-AKT1
P27KIP1
Cyclin E1
DNAJB6a
loading ctrl: p84
70 kDa
55 kDa
25 kDa
40 kDa
100 kDa

C

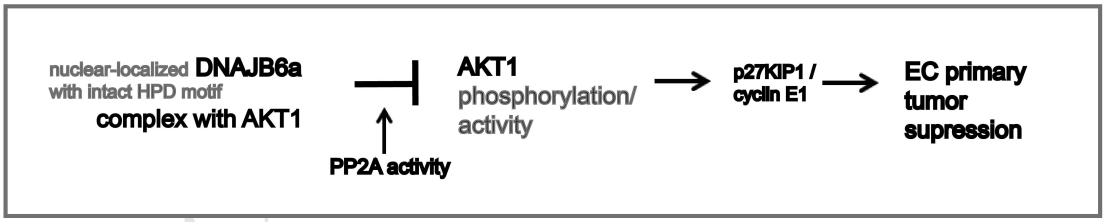
nuclear-localized DNAJB6a
with intact HPD motif
complex with AKT1
AKT1
phosphorylation/
activity
PP2A activity
p27KIP1 /
cyclin E1
EC primary
tumor
supression

Supplementary Materials and Methods

Tissue microarray (TMA) and immunohistochemical (IHC) staining

In this study two sets of TMAs from Hong Kong were utilized. All tumor specimens were obtained in Hong Kong Queen Mary Hospital from esophagectomies performed on patients, who had not received any pre-operative chemo-radiotherapy. Firstly, a total of 72 primary ESCC specimens collected from 1998 to 2005, together with 25 lymph node metastasis specimens from a subset of the 72 patients (Male/female=58/14; median age=63.5; T-stage $T_{1\text{-}2}/T_{3\text{-}4}$=13/59; N-stage $N_0/N_{1/2/3}$=47/25; M-stage M_0/M_1=62/10; Pathological-stage $p_{1\text{-}2}/p_{3\text{-}4}$=30/42; Grade-well/moderate/poor=11/42/19) from a previously constructed TMA were used.[1, 2] A second TMA is comprised of 88 primary ESCC specimens collected from 1991 to 1998 from 88 patients (Male/female=74/14; median age=65; $T_{1\text{-}2}/T_{3\text{-}4}$=7/81; $N_0/N_{1/2/3}$=52/36; M_0/M_1=86/2; $p_{1\text{-}2}/p_{3\text{-}4}$4=25/63; Grade-well/moderate/poor=28/43/17) and was constructed as described.[3] All samples were collected prospectively and consecutively. For TMA construction, collected samples were included randomly with balance of advanced and early stage samples.

IHC staining was performed and analyzed as previously described.[1, 2] DNAJB6 antibody (M01, Abnova, Taiwan) (1:100 dilution) was used as the primary antibody and recognizes both isoforms in Western blotting. Specific nuclear DNAJB6 staining intensity was examined and scored by two pathologists (KWC and AKYL), who were blinded as to the clinicopathological data of the patients. Cytoplasmic staining signal was not evaluated due to non-specific staining patterns as judged by both pathologists. The intensity of nuclear staining signal was scored using an arbitrary scale from 0 to 3, with negative (0), weak (1), moderate (2), and strong (3) expression levels, respectively. Scores of 0 and 1 were classified as low protein expression level and scores of 2 and 3 as high level. The sample size required for survival analysis was estimated to be minimally 95 (see “Sample size estimation” below for calculation); therefore, the results from both TMAs were pooled and analyzed together, as all samples were from Hong Kong patients in the same institute following the same collection protocol. See Supplementary Table 3 for summary. To evaluate the clinical relevance of *DNAJB6* in ESCC, IHC staining of two TMAs was performed and correlations of nuclear protein level were analyzed.

Chemical reagents

All chemical reagents used in this study were purchased from Sigma-Aldrich

Corporation (St. Louis, MO, USA) unless otherwise stated.

Cell lines

Sixteen ESCC cell lines, two immortalized esophageal epithelial cell lines, one immortalized nasopharyngeal epithelial cell line, and seven cell lines of other types of cancer were used (Supplementary Table 4).[4-20] KYSE30TSI was established from a subcutaneous tumor of a mouse injected subcutaneously with KYSE30. KYSE70TS was established from a tumor of a mouse injected subcutaneously with KYSE70.KYSE150Luc is a KYSE150 cell line labeled with firefly luciferase.[21] Cells were cultured as described.[22] Cells were routinely tested for mycoplasma contamination by both DAPI staining and PCR amplification of DNA.

Plasmids

The protein coding sequences from the plasmid pEGFP-N1-*DNAJB6a*WT (NCBI Reference Sequence: NM_058246.3), pIRES2-EGFP-HA-*DNAJB6*a-HPD(MUT) (mutated *DNAJB6a* in which the HPD motif, amino acids 31 to 33, were mutated to AAA), pIRES2-EGFP-HA-*DNAJB6*a-ΔJ (mutated *DNAJB6a*in which the DNAJ domain, amino acids 1 to 75, were removed), and the pRK5-Myc-*DNAJB6b*WT (NM_005494.2)were cut and ligated to corresponding vectors. The *DNAJB6a*-ΔNLS and *DNAJB6b*-ΔNES constructs were generated by fusion Polymerase Chain Reaction (PCR); the NLS sequence from amino acids 305 to 319 (KRKKQKQREESKKKK) of DNAJB6aand the NES sequence from amino acids 223-229 (LKSLTIN)of DNAJB6b were removed. In general, the pEGFP-N1 (Clontech, Mountain View, CA, USA) was used for subcellular localization study. The pWPI lentiviral expression vector (Addgene plasmid 12254) was used to express the gene of interest in cell lines. The pLKO.1 lentiviral shRNA vector (Addgene Plasmid 10878) was used for shRNA silencing in cell lines. Hairpin sequences targeting *DNAJB6* were obtained from The RNAi consortium (http://www.broadinstitute.org/rnai/public/). The pLKO.1 vector with non-targeting scrambled oligo (Addgene Plasmid 1864) served as a control for silencing studies. The lentiCRISPR genome engineering vector (Addgene Plasmid 49535) was used for protein expression interference assay in cell lines. Target genomic sequences and cloning primers were designed using CRISPR Design (http://crispr.mit.edu/). Non-targeting sgRNA (sequence: GTTCCGCGTTACATAACTTA) was used as negative control as described[23]. The primers for molecular cloning and sequences for shRNA and sgRNA are listed in Supplementary Table 5. A plasmid encoding myr-tagged AKT1 (Addgene Plasmid 46969) was used to express

constitutively active AKT1 in *DNAJB6a* over-expressing cells. For co-immunoprecipitation using anti-HA antibody, plasmids encoding HA-tagged DNAJB6 were generated by inserting the HA-tag coding sequence (TACCCATACGACGTCCCAGACTACGCT) at the N-terminus of *DNAJB6* in the pWPI-*DNAJB6* vectors.

Fusion PCR

Initial pre-fusion PCR reactions were performed using A/C primers set and B/D primers set for amplification of the sequences before the deletion and after the deletion, respectively, using the same annealing temperature 55ºC (see Supplementary Table 5 for primer identification). The two fragments were then gel-purified using QIAquick Gel Extraction Kit (Qiagen N.V., Venlo, Netherlands) and served as the templates for the following fusion PCR reaction, which was performed using A/B primers set and the two fragments purified as templates with the following cycles (95ºC 1', 50ºC 3', repeat 4 times) prior to regular PCR cycles (95ºC 30'', 55ºC 1', 72ºC 30'', repeat 30 times).

Lentivirus preparation and infection

For lentiviral infection, the pWPI vector containing the gene of interest, pLKO.1 vector containing the hairpin sequences, or lentiCRISPR vector containing targeted RNA sequences were used together with the packaging vector psPAX2 (Addgene plasmid 12260) and the envelope vector pMD2.G (Addgene plasmid 12259). The human embryonic kidney HEK293T cell line was used as the packaging cell line. The HEK293T cells were seeded overnight for transfection. The pWPI/pLKO.1/lentiCRISPR/pLVX-EF1a, psPAX2, and pMD2.G vectors were mixed in a ratio of 4:3:1 in weight (8μg/6μg/2μg) (for a tissue culture T-75 flask) and transfected using FuGENE HD transfection reagent (Promega, Madison, WI, USA) following the protocol from the manufacturer. Three DNAJB6a silencing oligos were used to transfect HEK293T cells all together to generate a pool of viruses containing all three oligos. Cells were kept three days without changing medium. The supernatant was then filtered using 0.45μm syringe filter (Pall, Port Washington, NY, USA). After infection, cells at passages 3~7 were used for assays.

Fluorescent fusion protein-based subcellular localization assay

Mutant forms of DNAJB6a/b were generated by fusion PCR as described above. The constructs were then fused to an enhanced green fluorescent protein at the C-terminal end using the pEGFP-N1 vector. The fusion proteins were transiently expressed in ESCC cell lines by DNA transfection using FuGENE HD transfection following manufacturer's protocol. The fluorescent signals indicating the subcellular localizations of the fusion proteins were

monitored and recorded using the Eclipse Ti florescent microscope (Nikon, Melville, NY) equipped with SPOT RT digital camera (Diagnostic Instruments, Inc., Sterling Heights, MI).

***In vivo* tumorigenicity assay**

Female BALB/c/nu/nu athymic nude mice (6-8 weeks of age) were obtained from the Laboratory Animal Unit of the University of Hong Kong. All experimental procedures were approved by the Committee on the Use of Live Animals in Teaching and Research in the University of Hong Kong. The tumorigenicity of cell lines was tested in nude mouse tumorigenicity assays. In general, cell numbers ($1x10^6$ for KYSE30TSI, $1.5x10^6$ for KYSE70TS, $1x10^7$ with 1:1 Matrigel (BD Bioscience, San Jose, CA, USA) for KYSE140, $5x10^6$ with 1:1 Matrigel for KYSE510, $4.5x10^6$ for KYSE450, and $5x10^6$ with 1:1 Matrigel for T.Tn), were injected subcutaneously into one flank of the mice, in a group of six mice per cell line. Tumor growth was monitored weekly by measuring the size using a caliper. Mice of the same group were culled and terminated if one of them developed severe tumor ulceration.

Experimental metastasis mouse model

For DNAJB6 metastasis assay, a total of $1x10^6$ KYSE150Luc cells with *DNAJB6a*/*b* over-expression were injected intravenously through the tail vein of female 6-8 weeks old athymic nude mice in a group of six mice per cell line. For TS1/TS2 metastasis assay, a total of $1.5x10^6$ cells were injected. Mice were then monitored by measuring bioluminescent signals using the Xenogen IVIS 100 System (PerkinElmer, Waltham, MA, USA) as described.[21] Mice survival data were also recorded.

RNA isolation and real-time quantitative PCR (QPCR)

RNA isolation, reverse transcription, and QPCR were performed as described.[24] For the Taqman assay for measuring expression of *DNAJB6a*, the gene-specific Taqman probe (Gene Expression Assay Hs00369717_m1, Applied Biosystems) was used. For the UPL QPCR assay for measuring *DNAJB6b*expression, forward primer (TGGCAGAAAAATCACTACAAAGAG) and reverse primer (TGCGTGCGTTGAATTACTTG) with UPL probe #68 (Roche Applied Science) were used. The Applied Biosystems® Human GAPD Endogenous Control (Invitrogen, Carlsbad, CA, USA) was used for equal loading control. Experiments were repeated three times independently. Expression with average fold-changes larger than 2 or smaller than 0.5 are considered altered.

Western blotting analysis

Western blot analysis was performed according to modified standard protocol

as described.[25] Antibodies used are listed in Supplementary Table 6.

Western blotting analysis on tumors from subcutaneous injection of mice

Cells were injected subcutaneously into nude mice. When tumors reached around 50-100mm^{3}in size, mice were killed and tumors were collected with minimal mice tissue contamination. Tumors were homogenized and lysed followed by procedures of Western blotting.

Flow cytometry cell cycle analysis

For synchronized G1/S transition regulation study, cells were seeded for 2 days and reached ~25-40 % confluence before incubation with serum-free medium for 72 hours to synchronize cells in the G1 phase. For synchronized G2/M transition regulation study, cells were seeded in culture flasks for 2 days before incubation with serum-containing medium with 2.5mM Thymidine for 24 hours. Cells were then released from the block for 3 hours by replacing with fresh serum-containing medium, followed by incubation with serum-containing medium with 50ng/mL nocodazole for 14 hours to synchronize cells in mitosis. Cells were then released by replacing with fresh medium. Flow cytometry analysis was performed as described.[26]

Cell proliferation assay

The proliferation and viability of cells were determined by the 3-(4,5-dimethylthiazol-2-yl)-2,5-diphenyltetrazolium bromide (MTT) assay as described.[27]

MTT proliferation assay with AKTi treatment

The Akt Inhibitor XIII (Merck Millipore, Darmstadt, Germany) was dissolved in dimethyl sulfoxide (DMSO) at a concentration of 13.3mM as stock. Cells were counted and seeded in triplicate in 96-well cell culture microplates. Fresh medium with 10% FBS and stated concentration of Akt inhibitor was added on Day 2. Measurements were taken on Day 4 as described above. Medium containing equally diluted DMSO was added to control cells.

Inhibitor assay

For Western blotting analysis, Akt Inhibitor was added into culture medium to the stated concentrations. Cells were seeded in 6-well plates overnight before incubation in Akt Inhibitor-containing medium overnight, followed by lysis preparation for Western blotting analysis. Medium containing equally diluted DMSO was added to control cells. For cellular sensitivity assessment, 3.5 μM Akt Inhibitor XIII for AKTi and 80 μM U0126 for MEKi were applied..

Insulin-like growth factor 1 (IGF-1) treatment

The recombinant human IGF-1 (PeproTech, Rocky Hill, NJ, USA) was added

into culture medium to the stated concentrations. Cells were seeded in 6-well plates overnight before incubation in IGF-1-containing medium overnight.

Okadaic acid treatment

Cells were seeded in 6-well plates over two nights and were incubated in 20μM okadiac acid for 1.5 hours before lysate collection. Medium containing equally diluted DMSO was added to control cells.

Near-infrared (NIR) fluorescent protein-based protein-protein interaction assay

The PAS/GAFm domains of iRFP were amplified from Addgene plasmids #39867 and #39868, respectively. A glycine-rich linker (DNA sequence: gga ggc ggg gga agc ggc gga ggc ggg tcc) was added to the C-terminus of PAS or the N-terminus of GAFm for further cloning. Constructs of protein pairs of interest, as indicated in text, were ligated to PAS/GAFm domains by fusion PCR, inserted into pLVX-EF1a (modified from pLVX-CMV, Clontech) lentiviral expression vector, and co-expressed by viral infections in KYSE30TSI cells. The pWPI vector encoding EGFP was co-expressed to mark the cell border. Live cell fluorescence images were acquired using the Carl Zeiss LSM 510 confocal microscopy (Oberkochen, Germany). The NIR fluorescent signal indicates the PAS and GAFm domains are present in close proximity, suggesting interaction/complexing between the two fusion proteins of interest. *AKT1*-wild type (WT) construct and *AKT1-MAA* mutant construct (K179M/T308A/S473A) were amplified from Addgene plasmids #9021 and #9031, respectively. The NIR fluorescence signal-positive cell percentage was calculated by averaging individual percentages (NIR-positive cell number/GFP-positive cell number) from 3 confocal microscopic images.

Co-immunoprecipitation (CoIP) assay

CoIP assay was performed according to the protocol from Abcam (Cambridge, UK) (http://www.abcam.com/protocols/immunoprecipitation-protocol-1), using non-denaturing buffer and recombinant protein G agarose (Invitrogen). Antibodies used are listed in Supplementary Table 6.

Microarray data analysis

Microarray data were downloaded from the GEO database (http://www.ncbi.nlm.nih.gov/geo/) using the accession number as indicated. Microarray data was extracted using MeV: MultiExperiment Viewer (http://www.tm4.org/mev.html).

Sample size estimation

The sample size required for the survival analysis using the Cox model was estimated using the formula shown below[28], where α is the rate of type I error

(significance level), β is the rate of type II error, 1-β is the power of the analysis, ϕ is the probability of the uncensored observation, p is the frequency of high expression of DNAJB6, and θ is the expected hazard ratio. In this study, the patient cohort had a death rate of 68.8% (ϕ=68.8%). We expected a hazard ratio of 0.5 (θ=0.5), a power of the analysis (1-β)=80%, and significance level α=0.05. The hazard ratio<1 is defined as the decrease of risk of death in the patients with high expression of DNAJB6 compared to the patients with low expression of DNAJB6. The total number of patients required for the analysis with 20%, 30%, 40% and 50% of high expression of DNAJB6 is 149, 113, 99, and 95, respectively.

$$N = \frac{\left(\mu_{1-\alpha/2} + \mu_{1-\beta}\right)^2}{(log\theta)^2 \varphi(1-p)p}$$

Statistical analysis

Statistical analyses for TMA were performed using the SPSS 19 statistical software package (IBM Corporation, Armonk, NY). Patient overall survival time was defined as the time elapsed from diagnosis to death with censoring of patients who died due to non-cancer related causes. Kaplan-Meier analysis was used for survival curves with log-rank tests for survival comparisons between groups. Univariate Cox proportional hazards model was applied to examine the association between overall survival and DNAJB6 expression, as well as other clinical parameters. In the multivariable survival analysis, factors that showed significant association with survival by the Kaplan-Meier analysis were included in the model. All the parameters were verified for the assumptions of the Cox model using R package.[29] The chi-square test was used for testing the association of nuclear DNAJB6 level with other clinical parameters. For other statistical analyses, the Student's t-test was used unless stated otherwise. A *p*-value less than 0.05 was considered statistically significant. All tests of significance were 2-sided. The error bars shown in the figures represent one standard deviation from the mean. For multiple-test comparisons, the *p* value was adjusted using false discovery rate method.[30] An adjusted *p*-value less than 0.05 is considered significant. An adjusted *p*-value less than 0.1 is considered marginally significant.

Supplementary Figure Legends

Supplementary Figure 1. Representative images of TMA DNAJB6 nuclear staining pattern in EC specimens. Scale: 400X.

Supplementary Figure 2. Kaplan-Meier survival analysis showed that presence of lymph node metastasis was a prognostic marker.

Supplementary Figure 3. Kaplan-Meier survival analysis showed that nuclear DNAJB6 level was a prognostic marker for better survival in patients without lymph node metastasis.

Supplementary Figure 4. Schematic diagram of *DNAJB6a* and *DNAJB6b*. The two variants differ in the very C-terminal. DnaJ: J-domain; G/F: Glycine-Phenylalanine Rich Region; NES: nuclear export signal; NLS: nuclear localization signal.

Supplementary Figure 5. Fluorescence microscopy imaging showed that WT DNAJB6a localizes to the nucleus, with the intact NLS and WT DNAJB6b diffuses through the cells, but becomes more nuclear when the NES is removed. Scale bar = 50 μm.

Supplementary Figure 6. Western blotting confirmed the expression of GFP-fusion mutant and WT DNAJB6a/b proteins in KYSE150 and KYSE30. Asterisk: bands indicating fusion protein expression.

Supplementary Figure 7.RNA expression profile of *DNAJB6a* and *DNAJB6b*in a panel of ESCC cell lines, as compared to immortalized normal esophageal epithelial cell line NE3. Only *DNAJB6a* expression is down-regulated in cancer cell lines compared to NE cells. The expression profile of NE083 was also provided as a reference.

Supplementary Figure 8. Tumor growth curves of the four EC cell lines over-expressing WT *DNAJB6a*/*b* and mis-localized *DNAJB6a* mutant in nude mouse tumorigenicity assay. Only WT nucleus-localized *DNAJB6a* over-expression suppresses tumor growth.

Supplementary Figure 9. Western blotting confirmed the expression of WT and mutant DNAJB6a/b proteins in the four cell lines for tumorigenicity assay.

Supplementary Figure 10. Tumor growth curves of the two EC cell lines with *DNAJB6a* silenced in nude mouse tumorigenicity assay. *DNAJB6a* silencing promotes tumor growth. ctrl: non-targeting control oligo.

Supplementary Figure 11. *In* vitro cell proliferation curves of KYSE510 and KSYE30TSI cells with WT and mutant *DNAJB6a*/*b* over-expression. Only WT nucleus-localized *DNAJB6a* over-expression suppresses cell proliferation.

Supplementary Figure 12. *In* vitro cell proliferation curves of KYSE450 and T.Tn cells with *DNAJB6a* silenced. *DNAJB6a* silencing enhances cell

proliferation. ctrl: non-targeting control oligo.

Supplementary Figure 13. Cell cycle progression after release from mitotic synchronization. *DNAJB6a* over-expressing KYSE30TSI cells or control cells progress toward G1 at a comparable rate. Recovery time: 2 hours.

Supplementary Figure 14. *In vitro* cell proliferation curves of KYSE450 and T.Tn with DNAJB6a expression interfered. Loss of DNAJB6a enhances cell proliferation. ctrl: non-targeting control oligo; sgRNA1 and sgRNA2: sgRNA specifically target *DNAJB6a*.

Supplementary Figure 15. *In vitro* cell proliferation curves of KYSE510 and KYSE30TSI with DNAJB6a expression and constitutively active AKT1 expression. Akt activity rescue greatly diminishes the inhibitory effect of DNAJB6a on cell proliferation. myrAKT: myr-tagged constitutively active AKT1 construct.

Supplementary Figure 16. Tumor growth curves of KYSE510 and KYSE30TSI cells over-expressing WT and mutant *DNAJB6a* in nude mouse tumorigenicity assay. Only over-expression of WT *DNAJB6a* with intact HPD motif suppresses tumor growth.

Supplementary Figure 17. *In* vitro cell proliferation curves of KYSE510 and KSYE30TSI cells with WT and mutant *DNAJB6a* over-expression. Only over-expression of WT *DNAJB6a* with intact HPD motif suppresses cell proliferation.

Supplementary Figure 18. Representative fluorescence images showing complexing of AKT1 and DNAJB6a *in vitro*. Co-expression of PAS-AKT1WT and DNAJB6a-GAFm fusion proteins produce NIR fluorescent signal, suggesting WT DNAJB6a complexes with WT AKT1. Introduction of either mutant (DNAJB6aAAA or AKT1MAA) fusion proteins diminishes the formation of complexes, as indicated by the absence of NIR signals (PAS-AKT1MAA/DNAJB6aWT-GAFM and PAS-AKT1WT/DNAJB6aAAA-GAFm). GFP signals show cell borders and NIR signals (red pseudocolor) indicate potential protein-protein interaction/complexing. Scale bar = 100 μm.

Supplementary Figure 19. Expressions of *DNAJB6a* transcripts in other cancer types. **: $P < .01$; n.s.: $P > .05$. All expression levels were normalized to that of the normal tissue for each cancer type, respectively. Data source: GSE1420 for EAC, GSE41804 for liver cancer, Bhattacharjee, A., *et al*.,[31] for lung cancer, GSE7803 for cervical cancer, and GSE32323 for colorectal cancer.

Supplementary Figure 20. Bioluminescent images of mice tail-vein injected

with *DNAJB6a*- over-expressing cells and vector-alone control cells. *DNAJB6a*- over-expressing cells show comparable lung colonization as the control cells.

Supplementary Figure 21. Bioluminescent intensities of mice tail-vein injected with *DNAJB6a*-over-expressing cells and vector-alone control cells. No significant differences were detected between the two groups.

Supplementary Figure 22. Survival curves of mice injected with *DNAJB6*-over-expressing cells and vector-alone control cells. Both groups of mice show comparable survival profiles.

Supplementary Figure 23. Co-immunoprecipitation assay confirming interaction between HSP70 and DNAJB6 in KYSE30TSI cells over-expressing HA-tagged DNAJB6. Anti-HA antibody was used to immunoprecipitate the HSP70/DNAJB6 complex. IP: immunoprecipitation; IB: immunoblotting; VA: vector-alone; Db: DNAJB6b; Da: DNAJB6a. Alpha-tubulin was used as a loading control and IP control.

Supplementary Table Legends

Supplementary Table 1. Interaction tests between nuclear DNAJB6 level and other prognostic clinicopathological parameters by Cox regression analysis.

Supplementary Table 2. Correlation analyses between nuclear DNAJB6 level and other clinicopathological parameters. *P*-value was calculated by Pearson Chi-square or Fisher's exact test, if values in any of the cells were below 5.

Supplementary Table 3. TMA clinicopathological parameters.

Supplementary Table 4. Cell lines used.

Supplementary Table 5. Primers and oligos used in molecular cloning.

Supplementary Table 6. Antibodies used.

Supplementary References

1. Yuen HF, Chan YP, Chan KK, et al. Id-1 and Id-2 are markers for metastasis and prognosis in oesophageal squamous cell carcinoma. Br J Cancer 2007;97:1409-15.
2. Chan SH, Yee Ko JM, Chan KW, et al. The ECM protein LTBP-2 is a suppressor of esophageal squamous cell carcinoma tumor formation but higher tumor expression associates with poor patient outcome. Int J Cancer 2011;129:565-73.
3. **Salajegheh A**, **Dolan-Evans E**, Sullivan E, et al. The expression profiles of the galectin gene family in primary and metastatic papillary thyroid carcinoma with particular emphasis on galectin-1 and galectin-3 expression. Exp Mol Pathol 2014;96:212-8.
4. Zhang H, Jin Y, Chen X, et al. Cytogenetic aberrations in immortalization of esophageal epithelial cells. Cancer Genet Cytogenet 2006;165:25-35.
5. Hu CP, Hsieh HG, Chien KY, et al. Biologic properties of three newly established human esophageal carcinoma cell lines. J Natl Cancer Inst 1984;72:577-83.
6. Mok CH, Chew EC, Riches DJ, et al. Biological characteristics of a newly established human oesophageal carcinoma cell line. Anticancer Res 1987;7:409-15.
7. Pan QQ. Studies on esophageal cancer cells in vitro. Proc Chin Acad Med Sci Peking Union Med Coll 1989;4:52-7.
8. Hu YC, Lam KY, Law SY, et al. Establishment, characterization, karyotyping, and comparative genomic hybridization analysis of HKESC-2 and HKESC-3: two newly established human esophageal squamous cell carcinoma cell lines. Cancer Genet Cytogenet 2002;135:120-7.
9. Shimada Y, Imamura M, Wagata T, et al. Characterization of 21 newly established esophageal cancer cell lines. Cancer 1992;69:277-84.
10. Tang JC, Wan TS, Wong N, et al. Establishment and characterization of a new xenograft-derived human esophageal squamous cell carcinoma cell line SLMT-1 of Chinese origin. Cancer Genet Cytogenet 2001;124:36-41.
11. Takahashi K KH, Chan C-T, Hosono, T, Takahara M, Sato K. A case of esophageal carcinoma metastatic to the mandible and characterization of two cell lines (T. T and T. Tn) established from the oral tumor. Japanese Journal of Oral and Maxillofacial Surgery 1990;36:307-316.

12. Lieber M, Smith B, Szakal A, et al. A continuous tumor-cell line from a human lung carcinoma with properties of type II alveolar epithelial cells. Int J Cancer 1976;17:62-70.
13. Scherer WF, Syverton JT, Gey GO. Studies on the propagation in vitro of poliomyelitis viruses. IV. Viral multiplication in a stable strain of human malignant epithelial cells (strain HeLa) derived from an epidermoid carcinoma of the cervix. J Exp Med 1953;97:695-710.
14. Glaser R, Zhang HY, Yao KT, et al. Two epithelial tumor cell lines (HNE-1 and HONE-1) latently infected with Epstein-Barr virus that were derived from nasopharyngeal carcinomas. Proc Natl Acad Sci U S A 1989;86:9524-8.
15. Kyriazis AP, DiPersio L, Michael GJ, et al. Growth patterns and metastatic behavior of human tumors growing in athymic mice. Cancer Res 1978;38:3186-90.
16. Jones PA, Laug WE, Benedict WF. Fibrinolytic activity in a human fibrosarcoma cell line and evidence for the induction of plasminogen activator secretion during tumor formation. Cell 1975;6:245-52.
17. Rifkin DB, Loeb JN, Moore G, et al. Properties of plasminogen activators formed by neoplastic human cell cultures. J Exp Med 1974;139:1317-28.
18. Rijken DC, Collen D. Purification and characterization of the plasminogen activator secreted by human melanoma cells in culture. J Biol Chem 1981;256:7035-41.
19. Schwartz AL, Fridovich SE, Knowles BB, et al. Characterization of the asialoglycoprotein receptor in a continuous hepatoma line. J Biol Chem 1981;256:8878-81.
20. **Li HM**, **Man C**, Jin Y, et al. Molecular and cytogenetic changes involved in the immortalization of nasopharyngeal epithelial cells by telomerase. Int J Cancer 2006;119:1567-76.
21. Li B, Tsao SW, Chan KW, et al. Id1-induced IGF-II and its autocrine/endocrine promotion of esophageal cancer progression and chemoresistance--implications for IGF-II and IGF-IR-targeted therapy. Clin Cancer Res 2014;20:2651-62.
22. Ko JM, Chan PL, Yau WL, et al. Monochromosome transfer and microarray analysis identify a critical tumor-suppressive region mapping to chromosome 13q14 and THSD1 in esophageal carcinoma. Mol Cancer Res 2008;6:592-603.
23. **Kearns NA**, **Genga RM**, Enuameh MS, et al. Cas9 effector-mediated

regulation of transcription and differentiation in human pluripotent stem cells. Development 2014;141:219-23.

24. Lo PH, Ko JM, Yu ZY, et al. The LIM domain protein, CRIP2, promotes apoptosis in esophageal squamous cell carcinoma. Cancer Lett 2012;316:39-45.
25. Lung HL, Bangarusamy DK, Xie D, et al. THY1 is a candidate tumour suppressor gene with decreased expression in metastatic nasopharyngeal carcinoma. Oncogene 2005;24:6525-32.
26. Lung HL, Cheung AK, Cheng Y, et al. Functional characterization of THY1 as a tumor suppressor gene with antiinvasive activity in nasopharyngeal carcinoma. Int J Cancer 2010;127:304-12.
27. **Leung AC**, **Wong VC**, Yang LC, et al. Frequent decreased expression of candidate tumor suppressor gene, DEC1, and its anchorage-independent growth properties and impact on global gene expression in esophageal carcinoma. Int J Cancer 2008;122:587-94.
28. Schoenfeld DA. Sample-size formula for the proportional-hazards regression model. Biometrics 1983;39:499-503.
29. R Core Team. R: A language and environment for statistical computing. R Foundation for Statistical Computing, Vienna, Austria. ISBN 3-900051-07-0, URL http://www.R-project.org/. 2013.
30. Benjamini Y, Hochberg Y. Controlling the False Discovery Rate - a Practical and Powerful Approach to Multiple Testing. Journal of the Royal Statistical Society Series B-Methodological 1995;57:289-300.
31. Bhattacharjee A, Richards WG, Staunton J, et al. Classification of human lung carcinomas by mRNA expression profiling reveals distinct adenocarcinoma subclasses. Proc Natl Acad Sci U S A 2001;98:13790-5.

Author names in bold designate shared co-first authors.

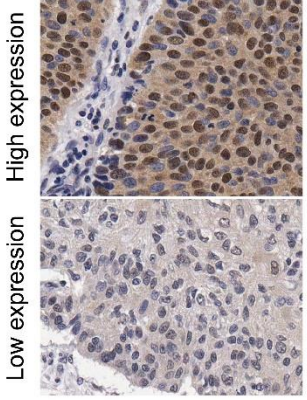

Supplementary Figure 1

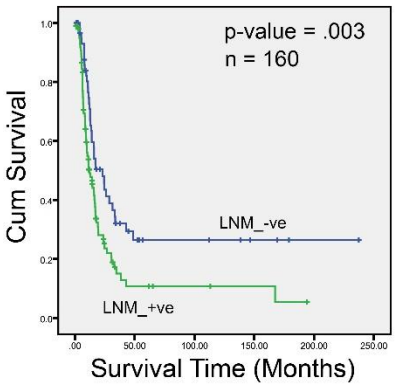

Supplementary Figure 2

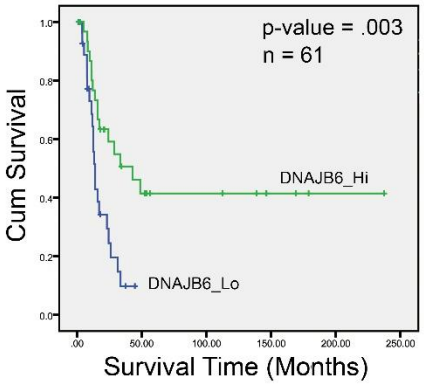

Supplementary Figure 3

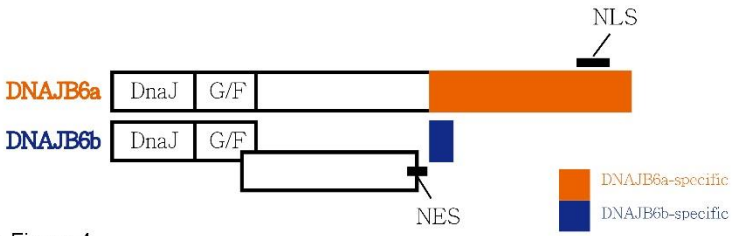

Supplementary Figure 4

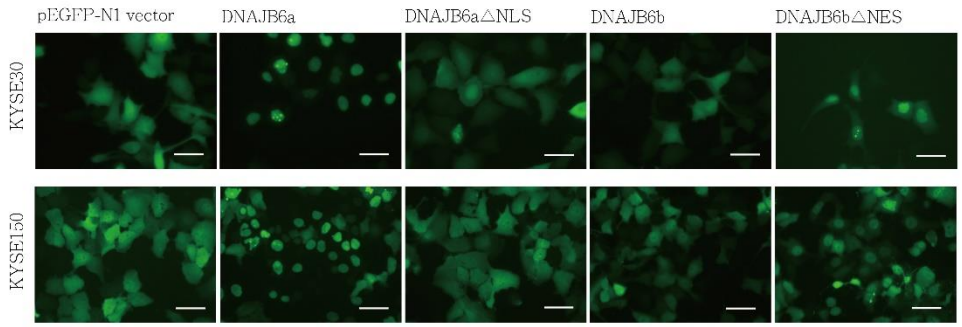

Supplementary Figure 5

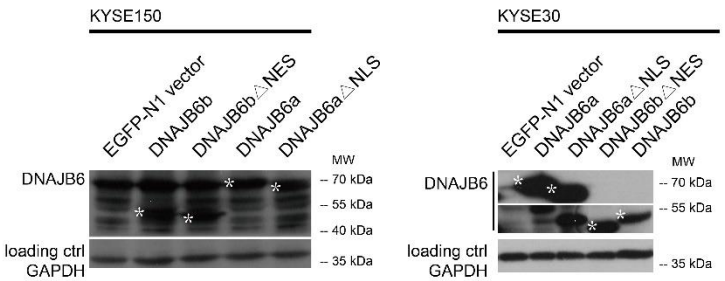

Supplementary Figure 6

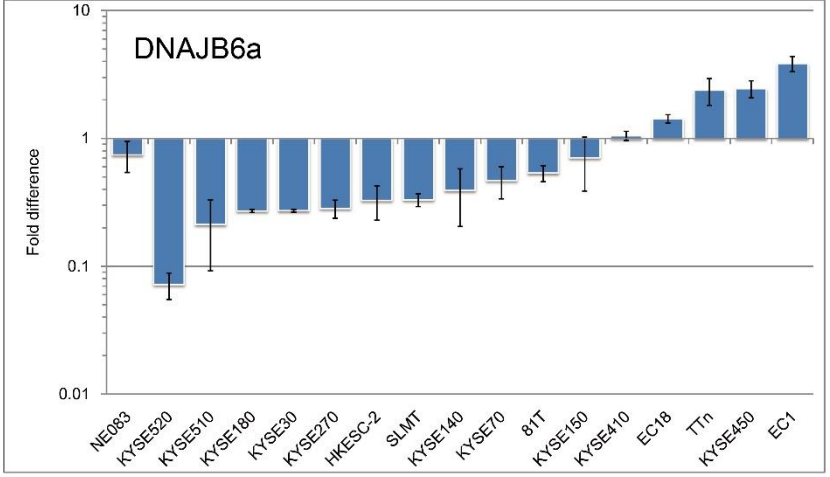

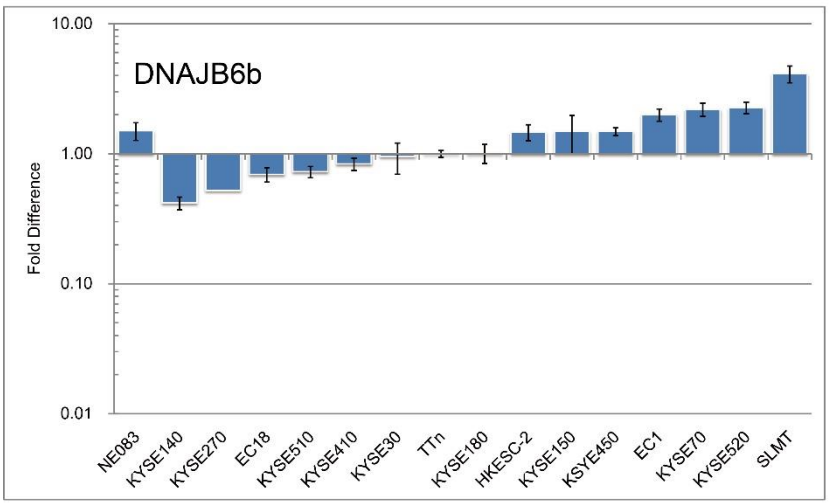

Supplementary Figure 7

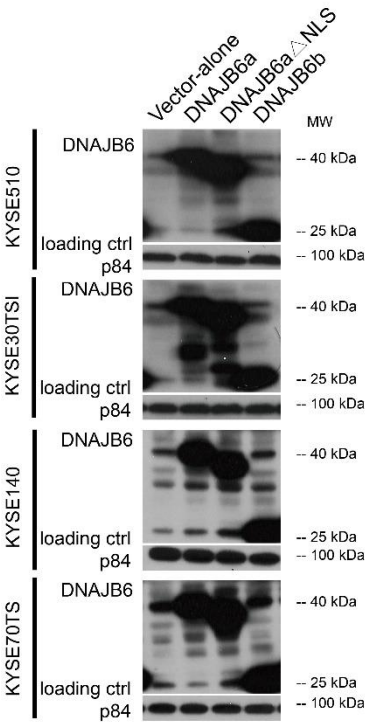

Supplementary Figure 9

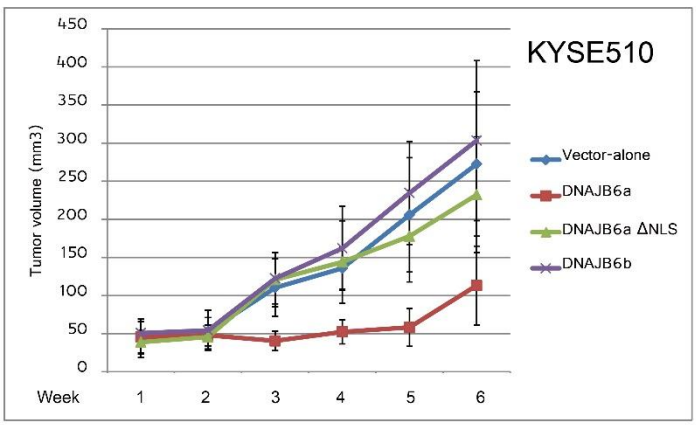

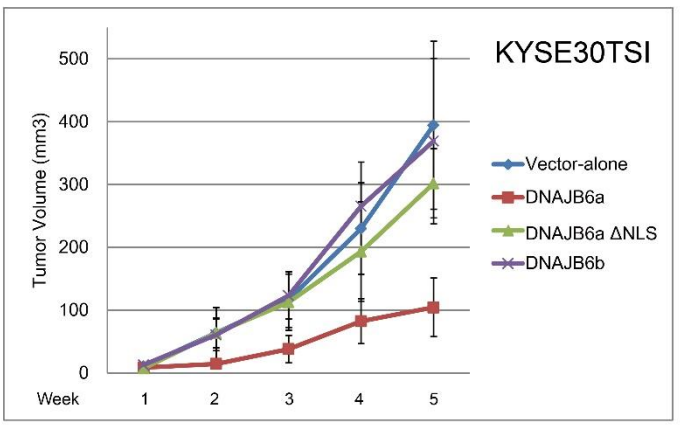

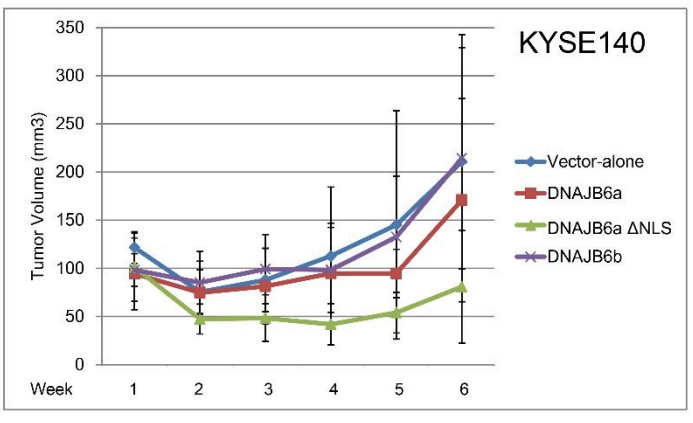

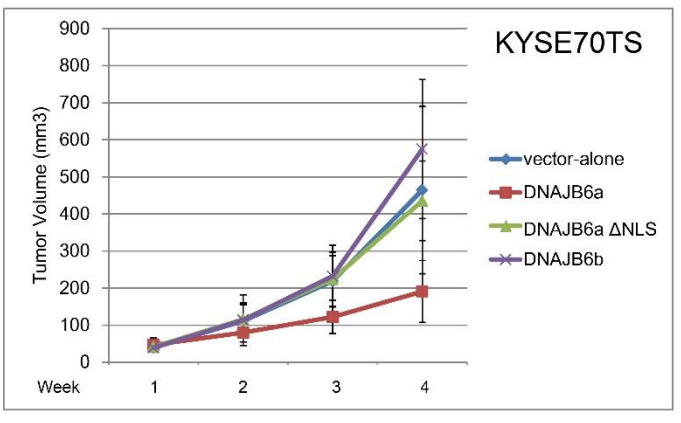

Supplementary Figure 8

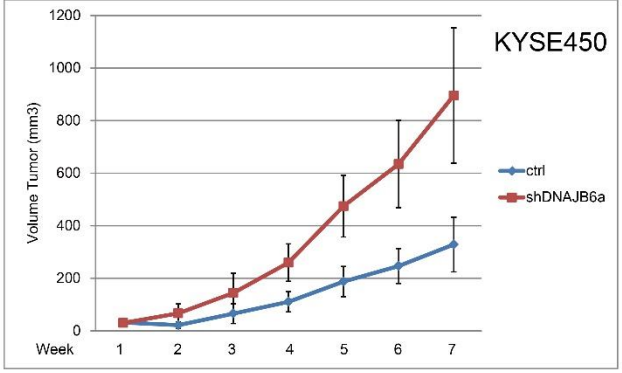

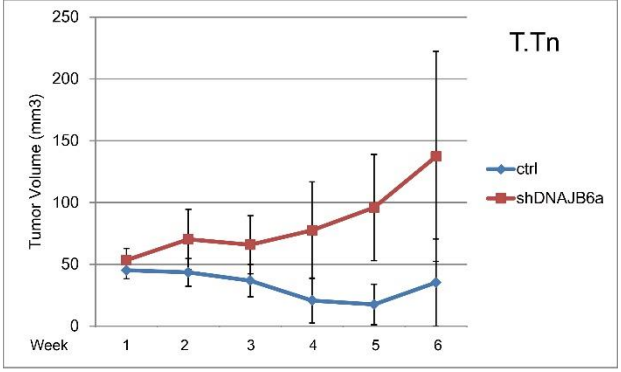

Supplementary Figure 10

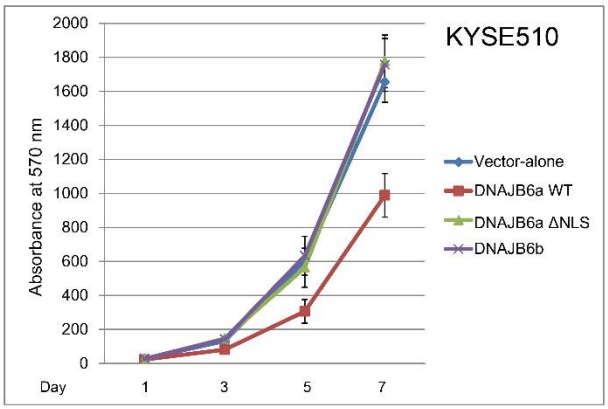

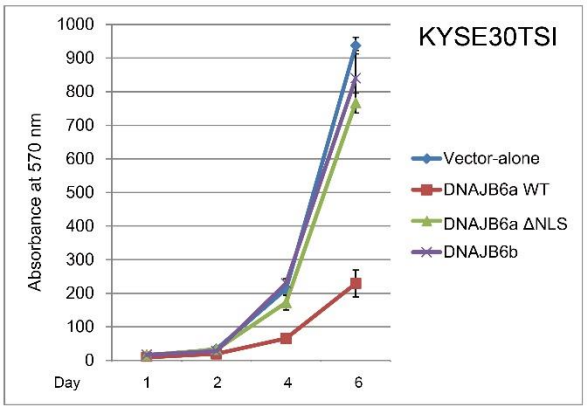

Supplementary Figure 11

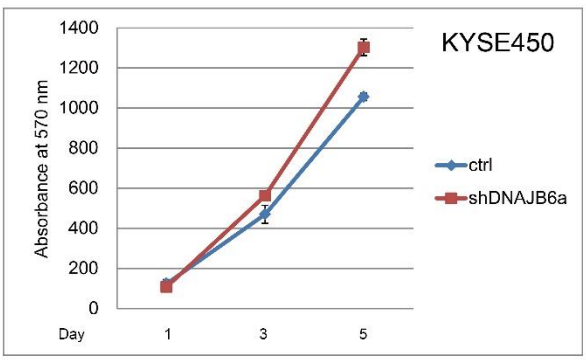

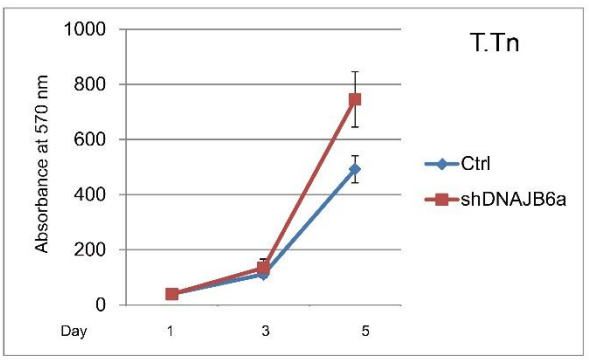

Supplementary Figure 12

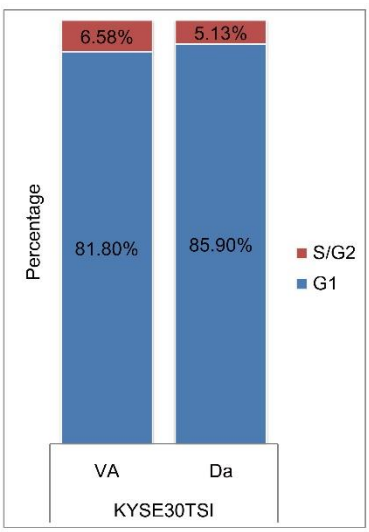

Supplementary Figure 13

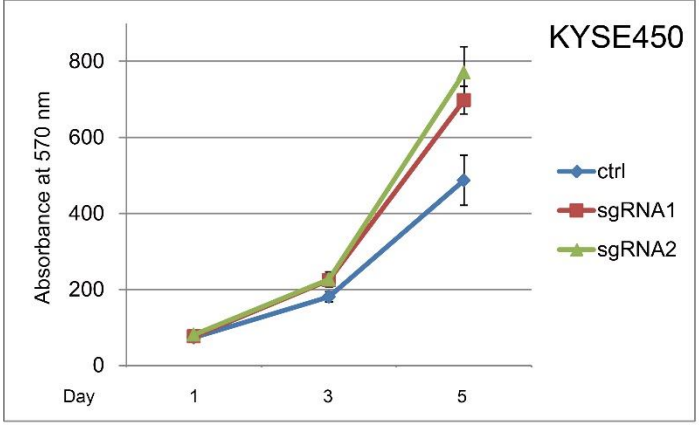

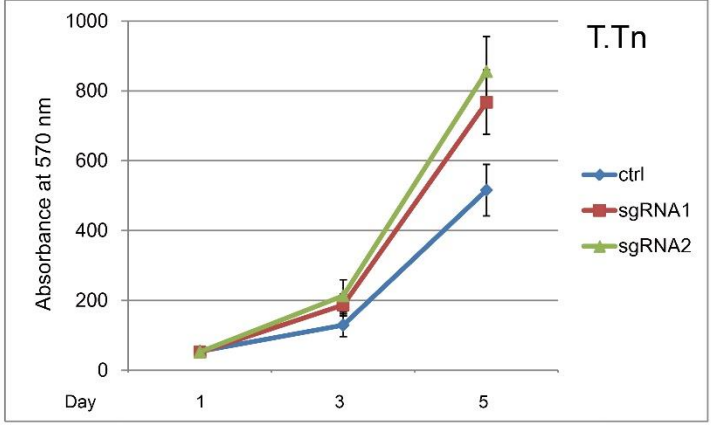

Supplementary Figure 14

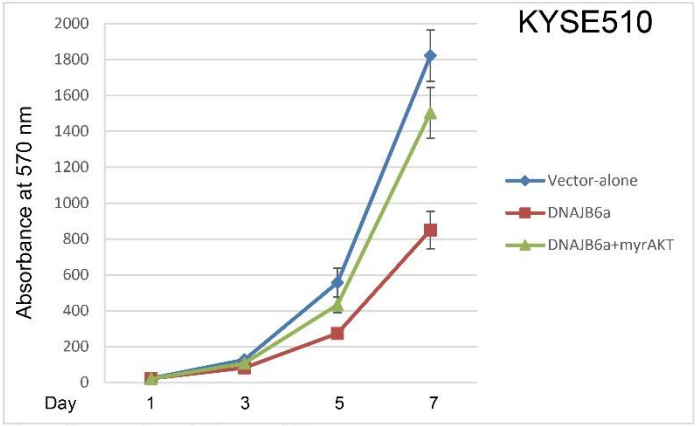

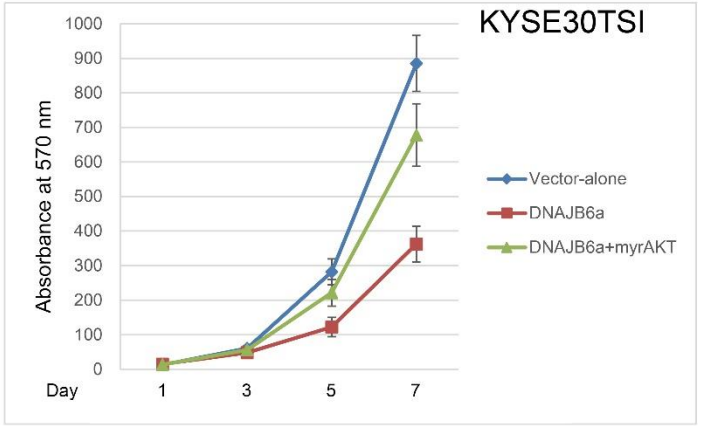

Supplementary Figure 15

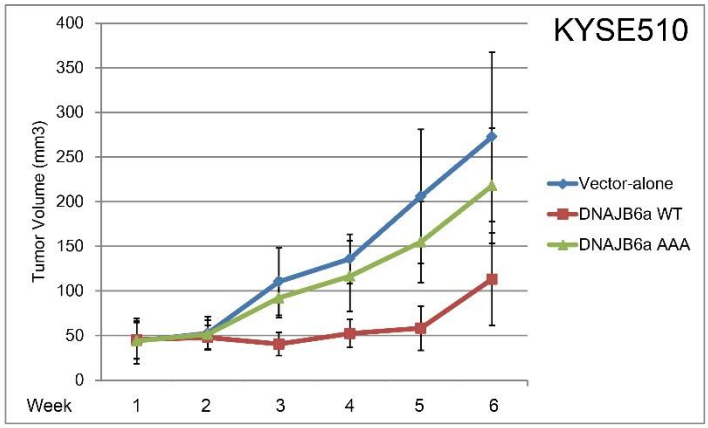

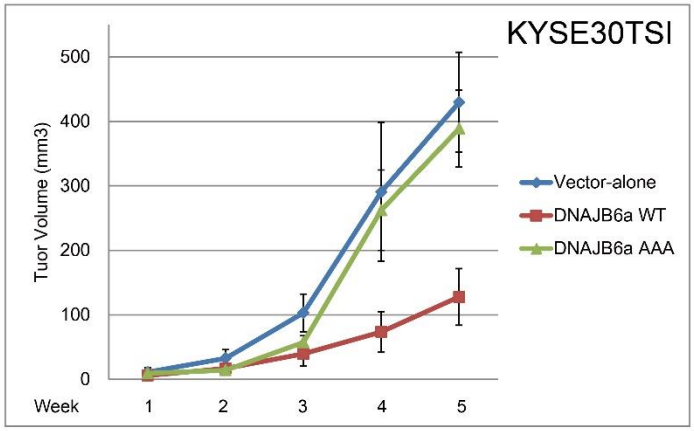

Supplementary Figure 16

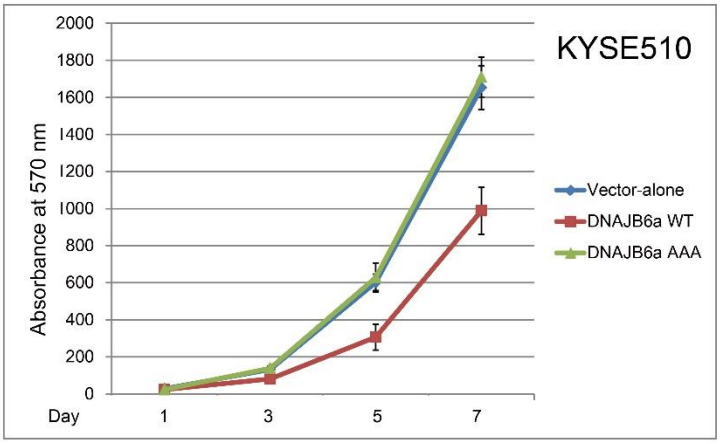

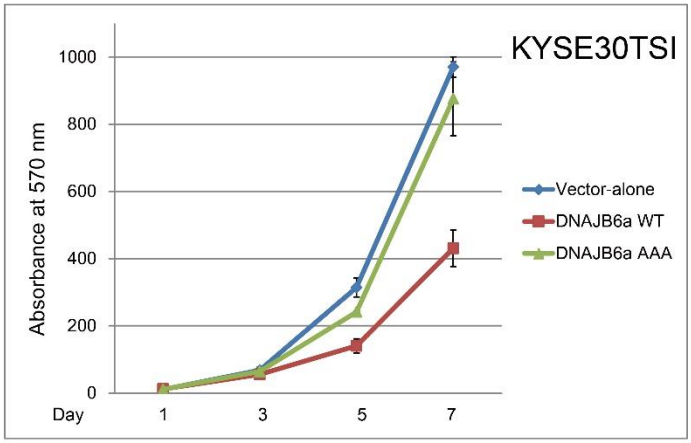

Supplementary Figure 17

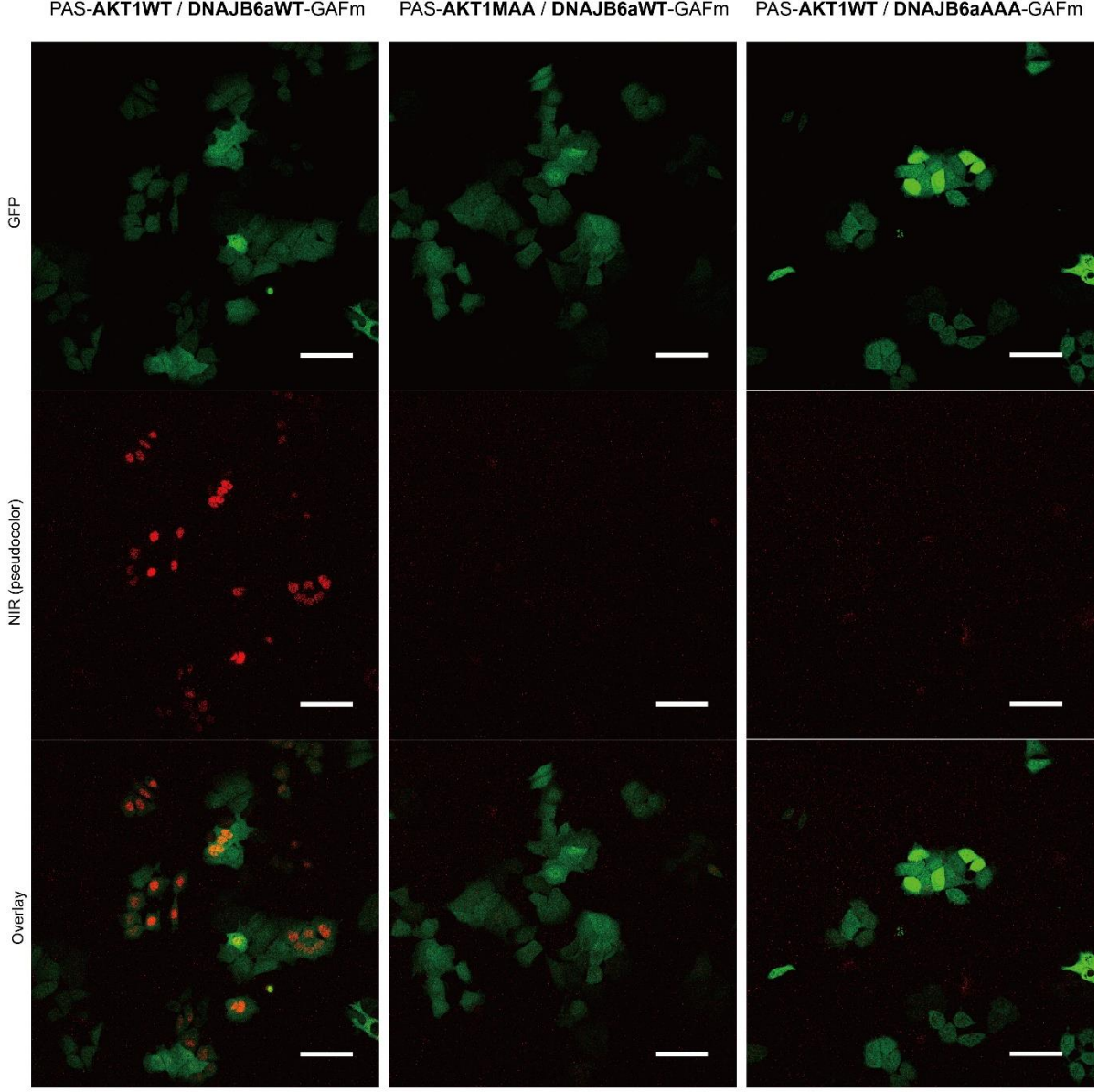

Supplementary Figure 18

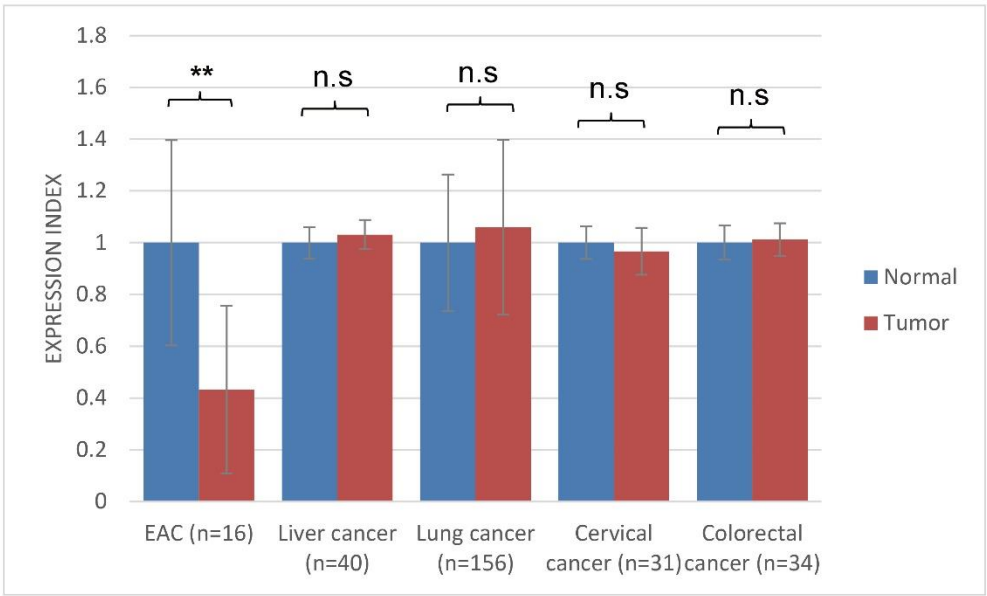

Supplementary Figure 19

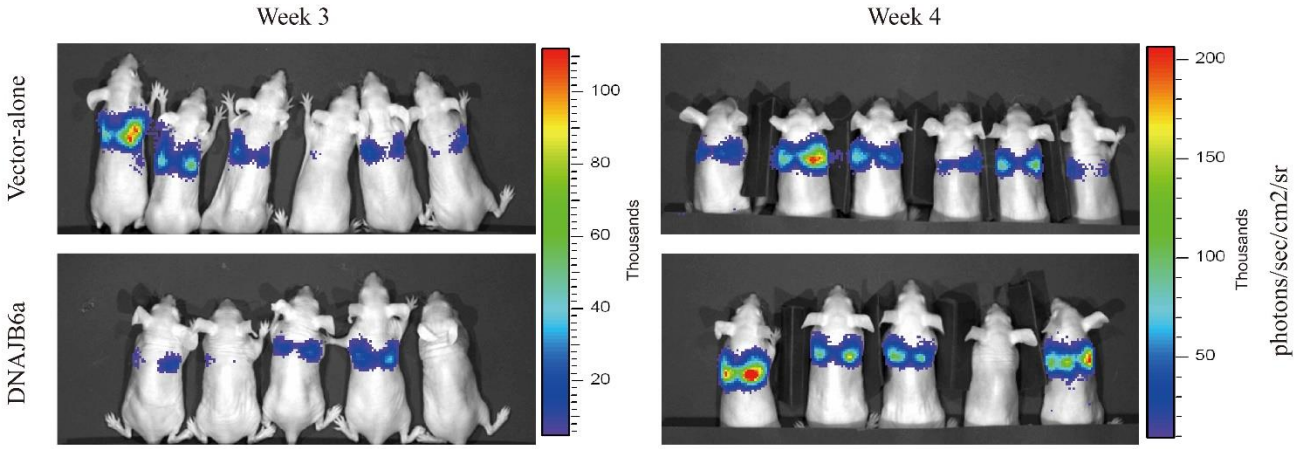

Supplementary Figure 20

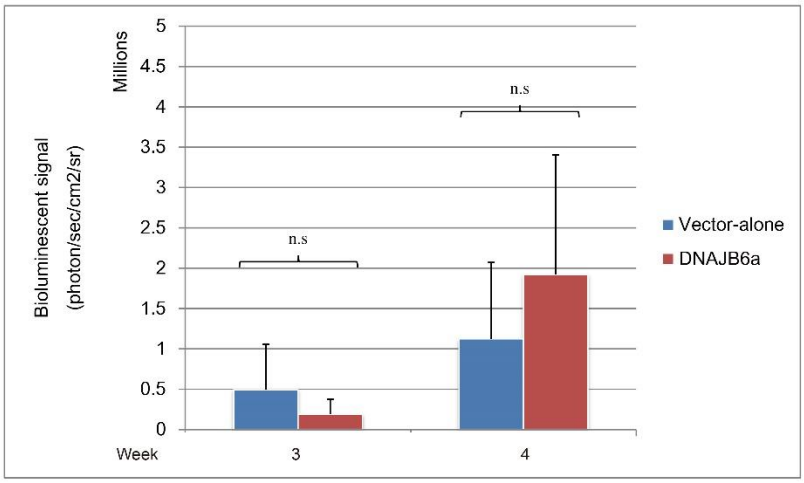

Supplementary Figure 21

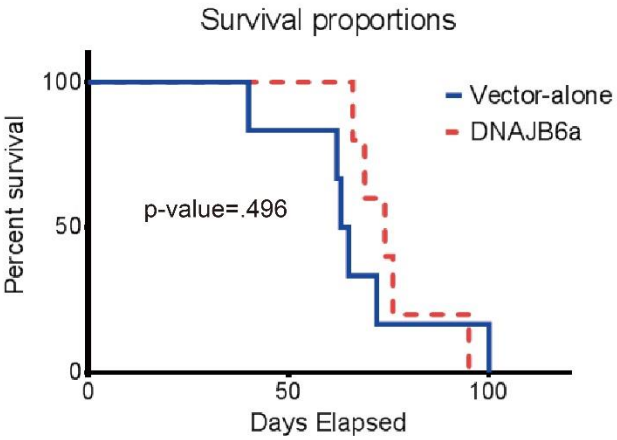

Supplementary Figure 22

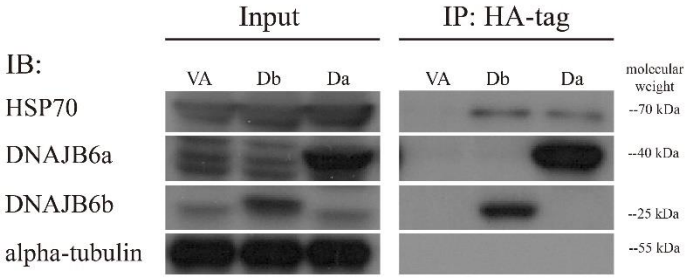

Supplementary Figure 23

	HR (95%CI)	*p*-value
DNAJB6 & Pathological stage		
DNAJB6	0.486 (0.237-0.999)	<.05
Pathological stage	1.767 (1.031-3.029)	.038
DNAJB6 x Pathological stage	1.370 (0.587-3.197)	.467
DNAJB6 & Lymph node metastasis		
DNAJB6	0.377 (0.195-0.731)	.004
Lymph node metastasis	1.137 (0.681-1.901)	.623
DNAJB6 x Lymph node metastasis	2.252 (1.001-5.066)	**<.05**
DNAJB6 & M stage		
DNAJB6	0.502 (0.332-0.760)	.001
M stage	1.014 (0.438-2.348)	.975
DNAJB6 x M stage	16.721 (4.110-68.025)	**<.0005**

Supplementary Table 1

	High nuclear DNAJB6 (No. / %)	Low nuclear DNAJB6 (No. / %)	*p*-value [#] (2-sided)
Lymph node metastasis			.**022**
positive	35/51.5	64/69.6	
negative	33/48.5	28/30.4	
Pathological stage			.242
I & II	27/39.7	28/30.4	
III & IV	41/60.3	64/69.6	
T stage			.630
T1 & 2	7/10.3	13/14.1	
T3 & 4	61/89.7	79/85.9	
M stage			.560
M0	64/94.1	84/91.3	
M1/1a/1b	4/5.9	8/8.7	
Grade			.129
G1 (Well-differentiated)	22/32.4	17/18.5	
G2 (Moderately differentiated)	32/47.1	53/57.6	
G3 (Poorly differentiated)	14/20.5	22/23.9	

#: calculated by Chi-squared test

Supplementary Table 2

	TMA1 (N = 72)[#] (No. / %)	**TMA2** (N=88)[#] (No. / %)	**Combined** (N=160)[#] (No. / %)
Gender			
Male	58/80.6	74/84.1	132/82.5
Female	14/19.4	14/15.9	28/17.5
Total	72	88	160
Age of onset			
Median age (range)	68.5 (41-87)	63 (39-83)	65 (39-87)
Tissue type			
Primary Tumor	72/74.2	88/100	160/86.5
Lymph node metastasis	25/25.8	0	25/13.5
Total	97*	88	185
T stage			
T1	2/2.8	4/4.6	6/3.8
T2	11/15.3	3/3.4	14/8.8
T3	45/62.5	60/68.2	105/65.6
T4	14/19.4	21/23.8	35/21.9
Total	72	88	160
M stage			
M0	62/86.1	86/97.7	148/92.5
M1	10/13.9	2/2.3	12/7.5
Total	72	88	160
Pathological stage			
I	0	7/8.0	7/4.4
II	30/41.7	18/20.5	48/30
III	32/44.4	61/69.2	93/58.1
IV	10/13.9	2/2.3	12/7.5
Total	72	88	160
Grade			
Well	11/15.3	28/33.0	39/24.4
Moderate	42/58.3	43/47.7	85/53.1
Poor	19/26.4	17/19.3	36/22.5
Total	72	88	160
Lymph node metastasis			
Positive	47/65.3	52/59.1	99/61.9
Negative	25/34.7	36/40.9	61/38.1
Total	72	88	160
Nuclear DNAJB6 staining			
Higher expression	53/73.6	39/44.3	92/57.5
Lower expression	19/26.4	49/55.7	68/42.5
Total	72	88	160

#: number of patients enrolled

*: total samples from 72 patients

Supplementary Table 3

Cell Line	Description	Culture medium
NE3	Immortalized normal esophageal epithelial cells	50% Defined Keratinocyte-SFM + 50% EpiLife®
NE083		
81-T	ESCC	Roswell Park Memorial Institute medium (RPMI) with 10% Fetal bovine serum (FBS)
EC1		RPMI with 10% FBS
EC18		
HKESC-2		Dulbecco's Modified Eagle medium (DMEM) with 5% FBS and 5% Newborn Calf Serum (NCS)
KYSE30		RPMI with 10% FBS
KYSE70		
KYSE140		
KYSE150		
KYSE180		
KYSE270		
KYSE410		
KYSE450		
KYSE510		
KYSE520		
SLMT-1		DMEM with 5% FBS and 5% NCS
T.Tn		RPMI with 10% FBS
A549	Lung adenocarcinoma	DMEM with 5% FBS and 5% NCS
BOWES	Melanoma	
HeLa	Cervix carcinoma	
HepG2	Hepatocellular carcinoma	
HONE-1	Nasopharyngeal carcinoma	
SW480	Colon adenocarcinoma	RPMI with 10% FBS
HT1080	Fibrosarcoma	DMEM with 5% FBS and 5% NCS
NP460	Immortalized normal nasopharyngeal epithelial cells	50% Defined Keratinocyte-SFM + 50% EpiLife®

Supplementary Table 4

DNAJB6 shRNA silencing oligos		
TRC clon	**Target sequence**	**Forward Sequence / Reverse Sequence**
TRCN0000293467	TCGATATCAACTTCAACTAAA	CCGGTCGATATCAACTTCAACTAAACT**GC**AGTTTAGTTGAAGTTGATATCGATTTTTG
		AATTCAAAAATCGATATCAACTTCAACTAAACT**GC**AGTTTAGTTGAAGTTGATATCGA
TRCN0000008778	CGGGACATCTATGACAAATAT	CCGGCGGGACATCTATGACAAATATCT**GC**AGATATTTGTCATAGATGTCCCGTTTTTG
		AATTCAAAAACGGGACATCTATGACAAATATCT**GC**AGATATTTGTCATAGATGTCCCG
TRCN0000293469	TGATTGTTGGGACCACATAAT	CCGGTGATTGTTGGGACCACATAATCT**GC**AGATTATGTGGTCCCAACAATCATTTTTG
		AATTCAAAAATGATTGTTGGGACCACATAATCT**GC**AGATTATGTGGTCCCAACAATCA

DNAJB6 CRISPR targeting oligos		
Target	**Genomic sequence**	**Forward Sequence / Reverse Sequence**
DNAJB6b	TAAGGAGCAGCTGCTGCGCT TGG	CACCG TAAGGAGCAGCTGCTGCGCT
		AAAC AGCGCAGCAGCTGCTCCTTA C
DNAJB6a	GCTGAGGAGCGCATGCGGAG AGG	CACCG TAAGGAGCAGCTGCTGCGCT
		AAAC AGCGCAGCAGCTGCTCCTTA C
DNAJB6a	GACCCCCTCGCGTCCGCAGC AGG	CACC GACCCCCTCGCGTCCGCAGC
		AAAC GCTGCGGACGCGAGGGGGTC

Cloning primers for DNAJB6 mutant constructs		
Construct	**Name**	**Primer Sequence**
DNAJB6a ΔNLS	N-terminus F (A)	GGAATTCGCCACCATGGTGGATTACTATGAAGTTCTA
	delNLS R (C)	GTGATTGCCTTTGGTCGAGCCACCTTCTTTCAATCCTGCT
	delNLS F (D)	GGATTGAAAGAAGGTGGCTCGACCAAAGGCAATCACTAG
	C-terminus R (B)	GGGATCCGCCACCCTAGTGATTGCCTTTGGTCGA
DNAJB6b ΔNES	N-terminus F (A)	GGAATTCGCCACCATGGTGGATTACTATGAAGTTCTA
	delNES R (C)	CAGCAGCTGCTCCTTACCCTGGCCATCTTCTTCAACTTCTAC
	delNES F (D)	GTTGAAGAAGATGGCCAGGGTAAGGAGCAGCTGCTGC
	C-terminus R (B)	CGGGATCCTTACTTGTTATCCAAGCGCAGC

Supplementary Table 5

Antibody target	Vendor	Catolog No.
DNAJB6	Genetex	GTX101947
p84	Genetex	GTX70220
GAPDH	Genetex	GTX100118
cyclin E1	Santa Cruz	sc-247
AKT1 T308 phosphorylation	Cell Signaling	#4056
AKT1 S473 phosphorylation	Cell Signaling	#4058
AKT1 total form	Cell Signaling	#9272
p27KIP1	Genetex	GTX100446
Rabbit IgG antibody (HRP)	Genetex	GTX213110-01
Mouse IgG antibody (HRP)	Genetex	GTX213111-01
Anti-HA antibody	Sigma-Aldrich	H3663
Alpha-tubulin	Genetex	GTX108784
HSP70	Genetex	GTX111088

Supplementary Table 6